

applied spectroscopy

Polymorph Characterization of Active Pharmaceutical Ingredients (APIs) Using Low-Frequency Raman Spectroscopy

**Peter J. Larkin,^{a,*} Marta Dabros,^b Beth Sarsfield,^{a,†} Eric Chan,^a James T. Carriere,^c
Brian C. Smith^{d,‡}**

^a Bristol-Myers Squibb Company, One Squib Dr., New Brunswick, NJ 08903 USA

^b Bristol-Myers Squibb Company, Route 206 and Province Line Rd., Princeton, NJ 08543 USA

^c Ondax, 850 E. Duarte Rd., Monrovia, CA 91016 USA

^d Princeton Instruments, 15 Discovery Way, Acton, MA 01720 USA

Polymorph Characterization of Active Pharmaceutical Ingredients (APIs) Using Low-Frequency Raman Spectroscopy

Peter J. Larkin,^{a,*} Marta Dabros,^b Beth Sarsfield,^{a,†} Eric Chan,^a James T. Carriere,^c Brian C. Smith^{d,‡}

^a Bristol-Myers Squibb Company, One Squibb Dr., New Brunswick, NJ 08903 USA

^b Bristol-Myers Squibb Company, Route 206 and Province Line Rd., Princeton, NJ 08543 USA

^c Ondax, 850 E. Duarte Rd., Monrovia, CA 91016 USA

^d Princeton Instruments, 15 Discovery Way, Acton, MA 01720 USA

Polymorph detection, identification, and quantitation in crystalline materials are of great importance to the pharmaceutical industry. Vibrational spectroscopic techniques used for this purpose include Fourier transform mid-infrared (FT-MIR) spectroscopy, Fourier transform near-infrared (FT-NIR) spectroscopy, Raman spectroscopy, and terahertz (THz) and far-infrared (FIR) spectroscopy. Typically, the fundamental molecular vibrations accessed using high-frequency Raman and MIR spectroscopy or the overtone and combination of bands in the NIR spectra are used to monitor the solid-state forms of active pharmaceutical ingredients (APIs). The local environmental sensitivity of the fundamental molecular vibrations provides an indirect probe of the long-range order in molecular crystals. However, low-frequency vibrational spectroscopy provides access to the lattice vibrations of molecular crystals and, hence, has the potential to more directly probe intermolecular interactions in the solid state. Recent advances in filter technology enable high-quality, low-frequency Raman spectra to be acquired using a single-stage spectrograph. This innovation enables the cost-effective collection of high-quality Raman spectra in the 200–10 cm^{-1} region. In this study, we demonstrate the potential of low-frequency Raman spectroscopy for the polymorphic characterization of APIs. This approach provides several benefits over existing techniques, including ease of sampling and more intense, information-rich band structures that can potentially discriminate among crystalline forms. An improved understanding of the relationship between the crystalline structure and the low-frequency vibrational spectrum is needed for the more widespread use of the technique.

Index Headings: Raman; Lattice modes; Low frequency; Crystal form; Polymorph.

INTRODUCTION

Active pharmaceutical ingredients (APIs) are capable of forming solids as crystalline or amorphous glasses. The various crystalline forms are composed of molecules arranged in a three-dimensional structure with a local pattern (i.e., structural unit or unit cell) that repeats periodically in all directions with a regular repeat distance that results in a well-defined lattice.¹ Polymor-

phism, the potential of a crystalline material to exist in different crystalline phases with different molecular arrangements and/or conformations, is of critical interest in the development of pharmaceutical solid dosage forms.² Variations in the crystalline forms of APIs may affect their physiochemical properties, which can significantly impact the therapeutic index, bioavailability, manufacturing processing, and marketability of the commercialized drug product. Furthermore, the crystalline form of an API is often a key parameter in defining the scope of a pharmaceutical products' patent protection. As a result, developing improved capabilities and analytical techniques to analyze pharmaceutical solid-state forms is of widespread interest.

Pharmaceutical systems feature various types of solid-state forms. Polymorphs are characterized by having an identical chemical composition, but exhibiting different solid-state structures. Solids can involve the API either as the sole component or included with other chemical entities.³ Examples of multicomponent solids are solvates, salts, cocrystals, and various combinations of these. Solvates, also referred to as pseudo-polymorphs, contain chemical entities that are generally regarded as solvents. Hydrates are specialized solvates and include water in their lattice structure. Active pharmaceutical ingredients can also be encountered in a charged state as a salt and include counterions. Last, cocrystals contain the API and additional chemical entities (called cofomers) that are solids at room temperature. Recent literature includes discussions of the classification of and terminology for these different solid-state forms.^{4,5}

Classical vibrational spectroscopic techniques, including mid-infrared (MIR), near-infrared (NIR), and Raman spectroscopies, provide a probe of both the molecular structure and local environments.⁶ The spectral region typical of conventional infrared (IR) and Raman spectroscopies occurs between 4000 and 400 cm^{-1} , which is characterized by fundamental vibrations that are dominated by intramolecular vibrational modes. These vibrations derive from the various functional groups in the molecule and provide molecular structural information. Because of the high structural specificity, the spectral region 1800–200 cm^{-1} is labeled the fingerprint region.⁷ The NIR, conventional IR, and Raman spectral regions provide an indirect probe of the crystalline structure due to their sensitivity to changes in the local functional-group environments. These techniques are

Received 22 October 2013; accepted 2 January 2014.

* Author to whom correspondence should be sent. E-mail: larkin.peter.j@gmail.com.

† Current address: Aptuit SSCI, West Lafayette, IN 47906 USA.

‡ Current address: PerkinElmer Inc., 75 Nicholson Lane, San Jose, CA 95134 USA.

DOI: 10.1366/13-07329

acknowledged to be important tools for the solid-state characterization of pharmaceutical drug substances and drug products.^{8,9} Some of the attributes that have made these popular as characterization techniques in the pharmaceutical industry include (1) rapid, nondestructive sampling, (2) little or no sample preparation, (3) suitability for process analytical chemistry,¹⁰ and (4) the capability to differentiate crystalline forms, including amorphous forms.^{8,9} Raman and near-IR spectroscopies have particular advantages for in-line solid-state characterization because they require no sample preparation and are easily coupled to fiber optic probes.

The vibrational spectrum below 200 cm^{-1} has been used far less because of the experimental challenges of measuring the far-infrared (FIR) and low-frequency Raman spectra. The IR and Raman spectra in the low-frequency region ($200\text{--}10\text{ cm}^{-1}$) derive from the collective translation, libration, and deformations of the molecular skeleton within the crystal lattice.¹¹ This provides a second fingerprint region that is correlated with the crystal structure of the molecule because lattice phonons are involved. The advent of terahertz (THz) pulsed spectroscopy has facilitated the routine measurement of high-quality FIR spectra, which are typically reported in terahertz rather than wavenumbers.¹¹ Raman spectroscopy has also benefited from recent improvements in technology that facilitate low-frequency Raman measurements.¹² New advances in ultra-narrow-band notch filter technology with volume holographic gratings enable the generation of high-quality, low-frequency Raman spectra using a relatively compact, easy-to-use, and cost-effective system.¹³ Low-frequency Raman spectroscopy has been used extensively in studies of inorganic systems,¹⁴ and more recently it has been applied to the characterization of solid-state pharmaceuticals.^{15–22} Most low-frequency vibrational spectroscopic studies performed on solid-state pharmaceuticals have used THz spectroscopy.^{8,11,23–26} Unlike in classical Raman and IR spectroscopy, for which an excellent understanding of the characteristic frequencies for functional groups exists,^{6,7} a similar understanding of the FIR and low-frequency Raman spectral region has not been developed for complex aromatic structures, which are typical for many APIs. However, computational methodologies are increasingly being applied to develop an understanding of the characteristic vibrations below 200 cm^{-1} of organic molecular solids.²⁷

Molecular crystals are distinguished by two types of vibrations: intramolecular vibrations (also known as internal molecular vibrations or modes) and external vibrations (also called intermolecular vibrations, lattice vibrations, or phonon modes).²⁸ Intramolecular vibrations are observed in the typical IR and Raman spectral region $4000\text{--}200\text{ cm}^{-1}$. External vibrations occur where many atoms or molecules in the crystal oscillate coherently about their equilibrium positions at the same frequency.^{14,28,29} These oscillating phonon modes are commonly depicted as vibrational waves propagating through the crystalline lattice. Because organic molecules have large masses and corresponding moments of inertia, their phonon modes are typically low in energy and the background thermal energy will populate the phonon states. In molecular crystals, these include both

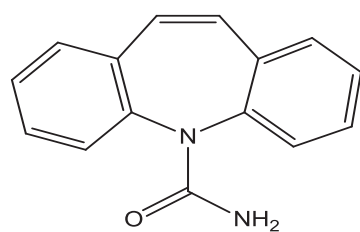
translational and rotational (librational) vibrations or mixed translation–libration vibrations. For larger organic molecules, the low-frequency spectral region below 200 cm^{-1} involves a combination of both intramolecular and external vibrations.^{28,29}

For materials that may exist as multiple crystalline polymorphs or pseudo-polymorphs, the low-frequency vibrational modes are particularly useful for the identification and characterization of each crystal form.^{14,18,22} Low-frequency IR and Raman bands are attributed to the lattice vibrational modes of the crystal and are dependent on the crystalline structure and the intermolecular forces between the molecules. Important intermolecular forces in solid-state aromatic APIs include hydrogen bonding and $\pi\text{--}\pi$ stacking interactions between aromatic rings. The corresponding spectral features are influenced by the crystal-packing arrangements and are unique to both the molecule and its crystalline environment.

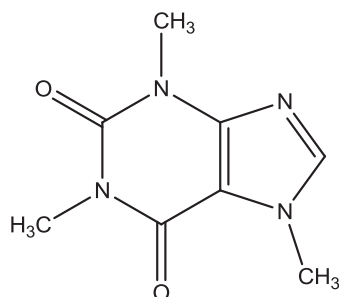
In this study, we demonstrate that the large aromatic molecules typical of many APIs have characteristic Raman bands below 200 cm^{-1} , deriving from both fundamental molecular vibrations and lattice vibrations. Furthermore, the aromatic APIs exhibit remarkably intense Raman bands below 200 cm^{-1} with complex spectral features. Similar intensities are not observed for most typical aliphatic pharmaceutical excipients, thus minimizing the spectral overlap in many pharmaceutical matrices. Low-frequency Raman spectroscopy easily discriminates between different crystalline forms and also provides a potential probe of the amorphous or disordered state of the API crystalline form in both the bulk API and drug products. Here we examine the low-frequency Raman spectra of three well-characterized APIs with rigid ring structures—carbamazepine (CBZ), theophylline, and caffeine—shown in Fig. 1. Carbamazepine is an anticonvulsant used to treat epilepsy and trigeminal neuralgia, theophylline is used mainly to treat bronchial asthma, and caffeine is commonly used as a stimulant. We also examine the low-frequency Raman spectra of a larger and more flexible molecule—apixaban—that has been developed by Bristol-Myers Squibb for the prevention and treatment of atrial fibrillation. This API has been demonstrated to crystallize in at least three different hemi-diacid isostructural cocrystals, as well as in a dihydrate and an anhydrous crystal form. Because the cocrystals of apixaban are isostructural, and thus can differ in chemical composition but adopt a similar arrangement of molecules within the crystal lattice, the molecules adopt the same symmetry and exhibit very similar molecular packing in the solid state

DESCRIPTION OF LOW-FREQUENCY VIBRATIONS

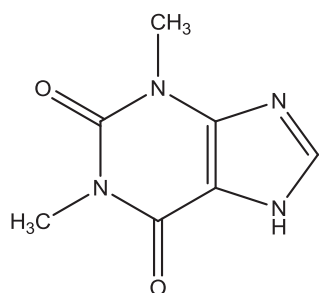
Considerable effort has been invested to better understand the optical spectroscopy and lattice dynamics of molecular crystals.²⁸ Much of the fundamental work has been applied to inorganic and simple organic molecular systems.^{14,28,29} Only recently have these experimental and theoretical tools been applied to the larger complex aromatic molecules characteristic of



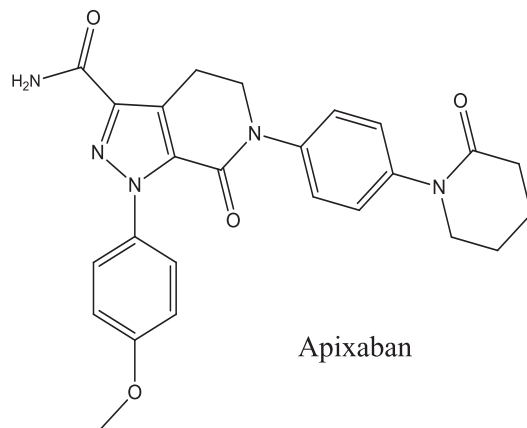
Carbamazepine



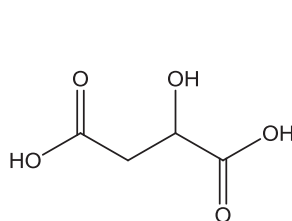
Caffeine



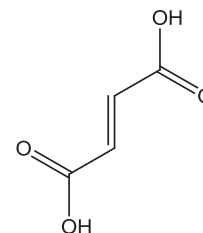
Theophylline



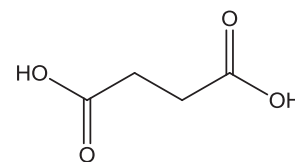
Apixaban



D,L-Malic acid



Fumaric acid



Succinic acid

FIG. 1. Chemical structures of the drug substances used in this study: CBZ; theophylline; caffeine; and the fumaric acid, succinic acid, and D,L-malic acid cocrystals of apixaban.

APIs.^{8,9,22,27,30} We first review a few fundamentals necessary to understand vibrational spectroscopy in the low-frequency spectral region.

Molecular crystals are characterized by vibrations as well as translational oscillations and rotational oscillations (librations), which are hindered by the crystalline structure.^{14,27–29} Typically, we consider the vibrational spectrum in terms of the molecular vibration (i.e., internal modes). The characteristic intramolecular and intermolecular vibrations observed in the low-frequency region vary as a function of the state of matter. The contributions to the spectrum from both types of vibration are greatest for molecules in the solid crystalline state and are considerably less for the amorphous, solution, and gas states. In the case of the external (lattice) intermolecular vibrations of the molecular crystal, the molecules as a whole are involved in quantized, coupled oscillations around their equilibrium positions in the periodic crystalline lattice. These external vibrations include both translational and rotational motions about their equilibrium positions. Analogous to intramolecular vibrations, the resulting lattice vibrations are a function

of both the molecular-site symmetry and the force constants (intermolecular forces) of the crystalline lattice.²⁸ This potentially enables the low-frequency IR and Raman spectral region to reliably differentiate among different polymorphic compounds.

As a first approximation in theoretical treatments of external vibrations of a crystalline lattice, we can treat the molecules as rigid blocks that can undergo translation, libration, or mixed translation–libration oscillations.^{27–29} The motions of the molecules in the crystal are coupled to form a wave in the crystalline lattice with a defined wavevector (\mathbf{K}) and frequency (Ω). Two types of phonon modes result: the acoustic phonons, which are IR and Raman inactive, and the optical phonons, which are IR and Raman active. For aromatic molecular crystals, the highest frequency of the optical phonons is expected at approximately 130 cm^{-1} (4 THz). The number of molecular vibrations has $3N - 6$ degrees of freedom, and there are $6Z - 3$ optical phonons, where N is the number of atoms in a molecule and Z is the number of molecules in a primitive unit cell.

Each phonon mode for a molecular crystal displays a dispersion relationship of the frequency (Ω) that is a function of the wavevector \mathbf{K} . The individual phonon-dispersion behavior (called a phonon branch) can be determined experimentally from inelastic neutron scattering. Because both IR and Raman spectroscopies measure the optical phonons with wavevectors of $\mathbf{K} \approx 0$, this dispersion is minimal. In addition, the acoustic phonon frequency vanishes at $\mathbf{K} \approx 0$ and, consequently, is not observed in IR and Raman spectra. However, because the IR and Raman techniques measure the optical phonons at $\mathbf{K} \approx 0$, they provide excellent tools to study the strong pressure and temperature dependence of low-frequency IR and Raman spectra that is typical of organic crystals.²⁹

In general, the intramolecular internal vibrational modes of the molecule occur at much higher frequencies than the phonon modes of the crystal.^{14,28,29} The classical 4000–400 cm^{-1} spectral region for the mid-IR and Raman spectra of organic molecules is dominated by intramolecular vibrational modes that are sensitive to changes in the local functional-group environments. Because the intermolecular coupling of the internal modes is typically extremely weak in the conventional spectral region, the molecular vibrational modes of each molecule in the crystal are considered to be excited independently. The lattice vibrations encountered in very low-frequency IR and Raman bands are characterized by significant intermolecular coupling. The solid-state crystalline arrangements of larger aromatic organic molecules exhibit low-frequency IR and Raman active molecular vibrations.^{22,27,30–32} The frequency of the low-energy molecular vibrations shifts to lower values with increasing molecular mass. This can result in the experimental separation between the intramolecular and the intermolecular (lattice) vibrations becoming less defined, and eventually, an overlap in the spectral region between the molecular and lattice modes can exist. In such cases, the influence of intermolecular coupling on the very low-frequency molecular vibrations can result in changes, such as the splitting of the bands associated with the molecular vibrations.²⁹ For larger organic molecules, this type of coupling can be observed in the region 200–100 cm^{-1} . The optical phonon modes of organic molecules are typically characterized by IR and Raman bands below 130 cm^{-1} .

One simple, very well-characterized example of an organic molecular system highlighting some of these points is anthracene.²⁹ The anthracene molecule is composed of 24 atoms and thus has $3 \times 24 - 6 = 66$ molecular vibrations. The observed frequencies for these internal molecular modes vary from 3108 to 111 cm^{-1} . The lowest vibrational mode (ω_{34}) is assigned to the “butterfly mode” (where the two rings bend in unison, mimicking a butterfly in flight) and is split into two bands at 129 and 111 cm^{-1} due to intermolecular coupling. The anthracene crystal unit cell contains two molecules and thus has $6 \times 2 - 3 = 9$ optical modes. In addition, it has three acoustic modes for a total of 12 external vibrations. The site-symmetry selection rules results in six Raman active modes and three IR active modes. For anthracene, there is an overlap between the low-frequency intramolecular vibrations and the external

lattice modes. In contrast, for smaller aromatic molecular crystals, such as naphthalene, a clear differentiation between the internal molecular modes and the external (lattice) modes is realized.

Spectroscopic techniques that are available to experimentally probe the phonon modes of crystalline materials include inelastic neutron scattering, and low-frequency Raman and THz spectroscopies. Inelastic neutron scattering provides the most comprehensive characterization of both the acoustic and optical phonon modes and their dispersion behavior, but instrumentation access is limited and the measurement and analysis are time consuming. The full characterization of the optical phonons of crystalline materials using vibrational spectroscopy requires both low-frequency Raman and THz spectroscopies because of the symmetry-based selection rules of these techniques. In general, low-frequency Raman spectroscopy is best for symmetric vibrations (A_g, B_g), and THz spectroscopy is best for asymmetric vibrations (A_u, B_u). Low-frequency Raman spectroscopy offers the significant advantage of minimal sample preparation and flexible experimental configurations for solid crystalline materials compared to THz spectroscopy.

EXPERIMENTAL

Materials. We fully characterized the crystal forms of CBZ, caffeine, theophylline, and apixaban using powder X-ray diffraction (PXRD). We then confirmed the crystal structures by comparing them to the predicted PXRD patterns derived from the single-crystal structure.[§] The unit cell parameters of the various crystal forms of CBZ, caffeine, theophylline, and apixaban used in this study are summarized in Tables SI–SIII.

Preparation of the Crystal Forms. Carbamazepine. Carbamazepine Form III (space group $P2_1/c$) (Tokyo Chemical Industry Co., Ltd.) was obtained and used as received. We prepared Form II (space group $R\bar{3}$) of CBZ by dissolving 1 g commercial CBZ Form III in 25 mL ethanol at 75 °C with continuous stirring. The solution was subsequently cooled to 4 °C and held for 7 h. The powder was isolated and dried at 50 °C. We prepared the dihydrate form ($P2_1/c$) of CBZ by suspending 1 g of the commercial CBZ Form III in a mixture of ethanol (10 mL) and water (15 mL) for 1 day. The solid was then filtered and dried at room temperature under vacuum (21 mm Hg partial pressure).

Apixaban. We prepared the cocrystals of apixaban (space group $P2_1/n$) by dissolving a total of 500 mg of 1:1.5 molar ratio of the drug and one of the acids (fumaric, succinic, or malic) in a mixture of ethanol (20 mL) and methanol (30 mL). For succinic acid, we used an excess quantity of acid to achieve the pure solid phase. The cocrystal solids were isolated by filtration after two days and dried at 50 °C.

Theophylline and Caffeine. Anhydrous materials of theophylline Form II (space group $Pna2_1$) (Spectrum) and caffeine beta form (space group $C2/c$) (Sigma-Aldrich) were obtained and used as received. We prepared the theophylline monohydrate (space group $P2_1/n$) by sus-

[§] For Figs. S1–S4 (confirmation of the crystalline forms) and Tables SI–SIII, see the Supplemental Material section.

pending 1 g of commercial theophylline in 5 mL water for 1 day. The isolated solid was filtered and dried at room temperature under vacuum (21 mm Hg partial pressure).

The polymorph identities and phase purities of the selected forms of CBZ, apixaban diacid cocrystals, theophylline, and caffeine were confirmed using powder XRD analysis and are summarized in Figs. S1–S4.

Instrumentation. Low-Frequency Raman Instrumentation. The Raman instrumentation and filter-enabling technology used in this study for the low-frequency Raman measurements have been described in greater detail elsewhere.^{12,13} Low-frequency Raman spectra were measured using 785.64 nm excitation, 180° backscattering geometry, and a spectral range that included both the Stokes and anti-Stokes scattering in the -144 to 703 cm^{-1} region. The instrument components included a IsoPlane™ SCT-320 Schmidt–Czerny–Turner spectrograph (Princeton Instruments, Acton, MA) with a 1200 grooves/mm holographic visible grating and a Pixis 2048 × 2048 back-illuminated charge-coupled device (CCD) camera (Princeton Instruments, Trenton, NJ) thermoelectrically cooled to -55 °C . The single-stage spectrograph was interfaced via a 25 μm diameter 0.1 numerical aperture (NA) step index (HJPSC25, ThorLabs) optical fiber to an XLF-CLM Raman sampling system (Ondax, Monrovia, CA) that included a SureLock 785 nm wavelength stabilized laser diode and a SureBlock XLF notch filter system arranged to collect 180° backscattered radiation from the powdered samples contained in nuclear magnetic resonance (NMR) tubes. This system provided a spectral resolution of 1 cm^{-1} over the entire frequency region.

We acquired the Raman scans for each sample with 12 exposures of 5 s each (12×5) and averaging for the final background-corrected spectra. This corresponds to a 1 min acquisition time using LightField acquisition software (version 4.4; Princeton Instruments). The Raman intensities are presented in relative units. The CBZ Form III band at 39 cm^{-1} resulted in 119 counts/s at 70 mW. The CCD analog-to-digital converter settings included a digitization rate of 100 kHz, a low-noise port, and a high-gain setting. The measured laser power at the sample was 70 mW. This was confirmed prior to each Raman measurement using a laser power meter (New Focus, model #3803).

Fourier Transform Raman Instrumentation. The FT-Raman measurements were made using a Nicolet 6700 FT-IR (Thermo Scientific) interfaced to a NXR FT-Raman module (Thermo Scientific) using a calcium fluoride (CaF_2) beamsplitter with a Raman NEXUS indium gallium arsenide (InGaAs) detector. A 180° Reflective Sampling Accessory (Thermo Scientific, part #840-0505000) was used to collect the backscattered Raman spectra. We transferred the powdered samples to an NMR tube, placed them in the NMR tube holder, and measured the FT-Raman spectra. The laser spot size specified by the vendor for these accessories was approximately 2 mm without the laser focusing lens. Prior to taking all the measurements, we optimized the FT-Raman system with sulfur at a laser power of 500 mW and auto-aligned it relative to the internal reference laser to ensure the accurate wavelengths of the Raman spectra. The FT-Raman measurements were made using vendor software, Omnic 8.2 (Thermo

Scientific). The spectra were measured at 4 cm^{-1} resolution with 256 scans, for a total measurement time of 4.5 min. The Raman intensities are presented in relative units.

Powder X-ray Diffraction Instrumentation. We performed the PXRD analysis at room temperature using a GADDS diffractometer (Bruker) equipped with manual chi platform goniometer and Hi Star detector with $\text{Cu K}\alpha$ radiation at wavelength 1.5418 Å. We placed samples in glass capillaries of 0.7 mm in diameter and rotated them during the data collection. Data were collected between 2° and 32° two-theta and integrated with a step size of 0.04° and a sample exposure time of 300 s.

Single-Crystal X-ray Diffractometry. We collected the single-crystal data using a AXS APEX2 CCD system (Bruker) and $\text{Cu K}\alpha$ radiation ($\lambda = 1.5418\text{ Å}$). The indexing and processing of the measured intensity data were carried out using the APEX2 software program suite.³³ The structures were solved by direct methods and refined on the basis of observed reflections using the SHELXTL software (Bruker).³³ The derived atomic parameters (coordinates and temperature factors) were refined using full-matrix least squares. The function minimized in the refinements was $\sum_w (|F_o| - |F_c|)^2$. R is defined as $\sum ||F_o| - |F_c|| / \sum |F_o|$ and $R_w = [\sum_w (|F_o| - |F_c|)^2 / \sum_w |F_o|^2]^{1/2}$, where w is an appropriate weighting function based on errors in the observed intensities, F_o are the experimentally measured observed factors and F_c are the calculated structure factors. Typically, all the non-hydrogen atoms were refined anisotropically and all H atoms were calculated using geometrical methods and refined using a riding model.

Software. Spectral Data Analysis. The Raman data were converted to the GRAMS format (*.SPC) and were analyzed using GRAMS/AI 7.02 (Thermo Scientific) and Excel 2007 (Microsoft).

Vibrational Analysis of Carbamazepine Dimer. Computational calculations were made using Materials Studio Software (version 5.5.3; Accelrys Software, Inc., San Diego). We used molecular mechanics methods to perform the vibrational analysis on a model for the dimer to characterize the observed frequencies. We obtained the molecular model for the H-bonded CBZ dimer to be used as a starting point for all the calculations from the crystal structure of CBZ Form II. We performed the vibrational analysis using the Discover module in Materials Studio Software (version 5.5.3; Accelrys Software Inc., San Diego), making use of the polymer consistent force field (PCFF), condensed-phase optimized molecular potentials for atomistic simulation studies (COMPASS) force field, and consistent valence force field (CVFF). The molecular coordinates were geometry-optimized with the respective force field prior to our calculation of the dynamical matrix, which was then diagonalized using the vibrational analysis tool of the Materials Studio Software graphic user interface (GUI). The geometries are optimized using the string matching algorithms research tool (SMART) algorithm with a quality setting of “ultra-fine.” The final energies for the dimer were -70.64 , -107.25 , and 174.55 kcal/mol for the PCFF, COMPASS, and CVFF optimizations, respectively.

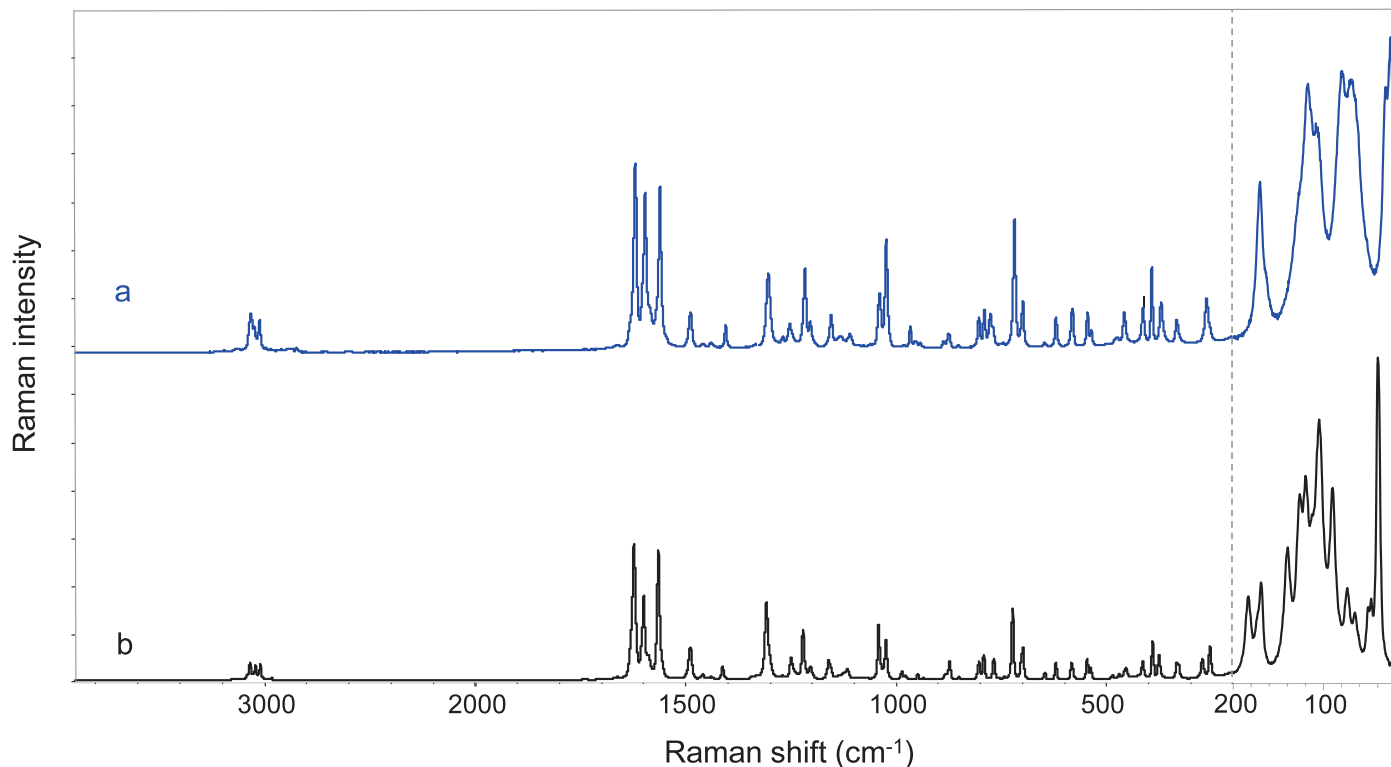


FIG. 2. High-frequency FT-Raman and low-frequency Raman spectra of two crystalline forms of CBZ. (**a**) Form II. (**b**) Form III. The frequency axis has been expanded for clarity and includes a 1× expansion in the region 4000–2000 cm^{-1} , a 2× expansion in the region 2000–200 cm^{-1} , and a 4× expansion in the region 200–20 cm^{-1} . The two, separately measured, high- and low-frequency spectra were spliced together by matching the intensities using Raman bands common to both in the 700–150 cm^{-1} spectral region.

RESULTS AND DISCUSSION

Comparison of Conventional and Low-Frequency Raman Spectra of Carbamazepine.

The Raman spectra of CBZ Forms II and III from 3800 to 10 cm^{-1} are shown in Figs. 2a and 2b. The spectra are a composite of the FT-Raman spectra acquired using 1064 nm excitation in the region 3800–200 cm^{-1} and the low-frequency Raman spectra acquired using 785 nm excitation in the region 200–10 cm^{-1} . The relative intensities of both the conventional (4000–400 cm^{-1}) and low-frequency (200–10 cm^{-1}) spectra were maintained using the overlapping spectra from both measurements in the 700–150 cm^{-1} spectral region. The wavenumber axis of the two fingerprint regions was expanded to facilitate comparison of the spectral features. A 2× frequency expansion was used in the fingerprint region (2000–200 cm^{-1}), which derives from vibrations from intramolecular vibrational modes, and a 4× frequency expansion was used in the low-frequency (200–10 cm^{-1}) spectral region, which includes external (lattice) intermolecular vibrations of the molecular crystal.

A comparison of the conventional and low-frequency Raman spectra of crystalline CBZ reveals that the band clusters below 200 cm^{-1} exhibit greater intensity and clearly differentiate between the two crystalline forms. Raman active vibrations are characterized by a change in the molecular polarizability (or deformation of the electron cloud) with respect to the vibrational mode. The Raman scattering intensity is related to the change in the polarizability tensor. The large intensities we observe associated with the Raman bands below 200 cm^{-1}

indicate a dramatic change in the polarizability for these low-frequency vibrations. Such large relative Raman intensities for low-frequency bands have been previously reported for alkyl-substituted benzenes.³⁴ There the strong Raman intensities were assigned to the σ - π interactions between the alkyl substituent and the benzene ring, which are modulated in selected ring bending and substituent torsional modes. Analogously, the large observed low-frequency Raman intensities for CBZ may derive from changes in the σ - π back-bonding between the primary amide and the aryl groups during these low-frequency vibrations.

The low-frequency Raman spectra of crystalline CBZ are characterized by a spectral fingerprint that is unique to the two solid-state crystalline forms. In contrast, the Raman bands in the higher-frequency region of the two forms of CBZ derive from the structurally specific intramolecular vibrations that are perturbed by the environmental differences between the two crystalline forms. Although differences between the higher-frequency Raman spectra of the two crystalline forms are present, they are not as pronounced as those we observed in the low-frequency region.

Low-Frequency Raman Spectra of Carbamazepine in Solution and the Calculated Vibrational Modes.

The contributions of intramolecular vibrations in the low-frequency region can be determined by measuring the low-frequency Raman spectrum of the API in the solution state. This approach requires the selection of a solvent that provides the API with a high solubility. Coupled with normal-mode analysis, the contributions from various

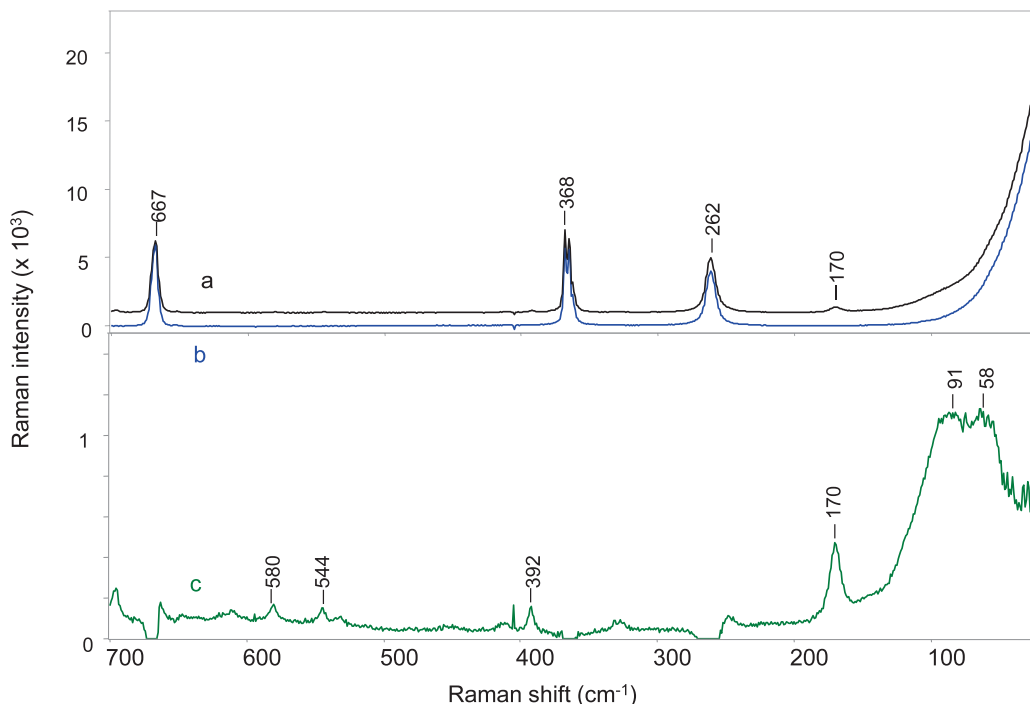


FIG. 3. (a) Low-frequency Raman spectrum of CBZ dissolved in chloroform (black spectrum); the concentration of the CBZ in chloroform solution was 100.5 mg/mL. (b) Low-frequency Raman spectrum of pure chloroform (blue spectrum). (c) Subtraction spectrum (green spectrum) showing Raman bands due to the molecular vibrations of CBZ.

functional groups can also be evaluated. The increased complexity and narrower bandwidths observed in the low-frequency Raman spectra of the solid state relative to the solution state derive from the lattice modes present only in the solid crystalline state. Experimental interference from solvent low-frequency Raman bands deriving from quasi-elastic light scattering and the Boson peak occur.³⁵

The low-frequency Raman spectra of CBZ in chloroform at a concentration of 100.5 mg/mL and of chloroform alone are shown in Figs. 3a and 3b. Chloroform has strong molecular vibrations at 667, 368, 365, and 262 cm^{-1} and a very strong low-frequency band observed below 80 cm^{-1} that derives from quasi-elastic light scattering and translational motions, possibly from micro-ordering effects.^{36,37} A distinct band from CBZ is clearly observed at 170 cm^{-1} . Figure 3c shows the CBZ solution subtraction spectrum, which minimizes the chloroform contributions. The measured Raman spectrum of CBZ in solution in spectral region 700–200 cm^{-1} has features similar to the solid-state spectra shown in Fig. 2. The solid-state crystalline forms of CBZ are characterized by a hydrogen-bonded dimer involving the primary amide group.²⁴ This same hydrogen-bonded dimer will form at the high concentration of CBZ in chloroform used here and is responsible for some of the similarities between the high-frequency Raman spectra of the solid and solution states.

We observe three major low-frequency Raman bands in the difference spectrum, at 170, 91, and 58 cm^{-1} , with a shoulder at 118 cm^{-1} for the CBZ in chloroform solution. The intense broad chloroform solvent band below 50 cm^{-1} precludes observation of any other possible low-frequency CBZ bands and affects the

quality of the spectral data below 100 cm^{-1} . All the observed solution-state CBZ low-frequency bands demonstrate a much greater intensity than are observed in the higher-frequency ($> 200 \text{ cm}^{-1}$) spectral region. This significantly increased intensity of the low-frequency Raman bands relative to the higher-frequency bands is analogous to that observed in Fig. 2 for the solid state. Because of the lack of external (lattice) vibrations and intermolecular coupling with a solid-state crystal lattice, the low-frequency Raman spectra of CBZ in solution is much simpler, with correspondingly broader bands, than the spectra of the solid crystalline state.

The calculated forms of the low-frequency molecular vibrations in the 200–55 cm^{-1} region for the hydrogen-bonded CBZ dimer are summarized in Fig. 4. These vibrational modes are suitable for the CBZ solution because of the calculated intramolecular vibrations and do not include the calculated external (lattice) vibrations. All the vibrations for the observed low-frequency bands in the 200–50 cm^{-1} region for CBZ in solution involve an out-of-plane ring bend (deformation) or fold and a separate primary amide out-of-plane bend/shear/twist or in-plane rock. A standing-wave methodology^{6,38} was used to describe the complex ring vibrations depicted in Fig. 4. The dashed lines depict the nodes that separate the two directions of the movement of the aromatic ring atoms. The number of nodes (dashed lines) observed in a given type of molecular vibration is directly related to the observed frequency. In general, the greater the number of nodes, the higher the frequency. Thus, the quadrant-fold ring vibration mode depicted in Fig. 4a has a calculated frequency of 170 cm^{-1} and the trigonal-fold modes (Figs. 4d and 4e) occur in the region 100–50 cm^{-1} . Similarly, the sextant and quadrant out-of-plane aromatic

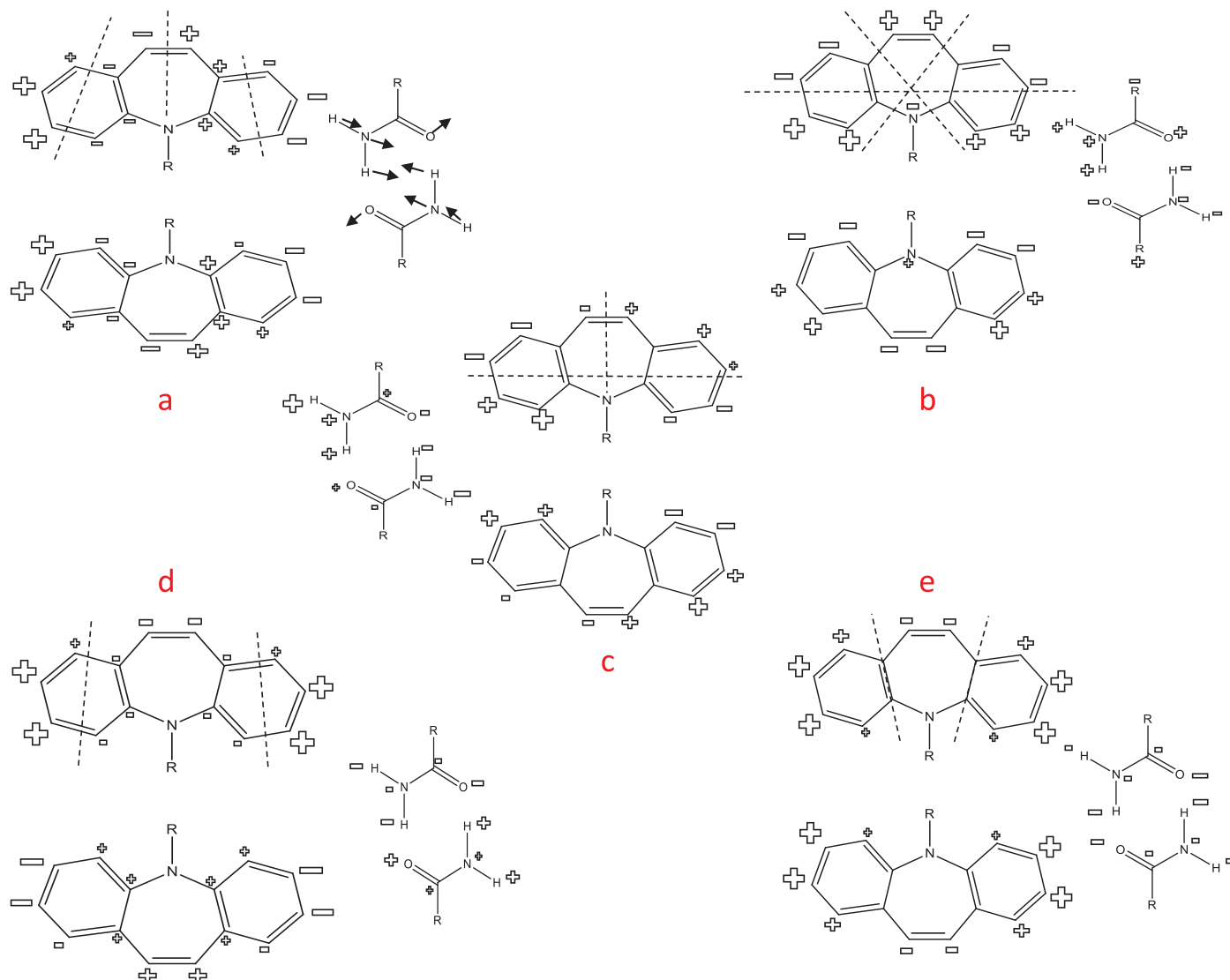


FIG. 4. Depiction of selected normal-mode vibrations of CBZ dimer in the low-frequency Raman region 200–55 cm^{-1} . A standing-wave description is used for the aromatic bending and folding vibrations where the nodes are highlighted with dashed lines. Negative signs depict atoms moving into the plane, and positive signs depict atoms moving out of the plane toward the viewer. The arrows depict atoms moving in the plane. The five vibrational modes are shown from highest to lowest calculated frequency. (a) Aromatic ring system quadrant out-of-plane fold (one-quarter accordion fold), dimer in-phase + primary amide dimer out-of-phase, in-plane rock. (b) Aromatic ring system sextant out-of-plane bend, dimer out-of-phase + primary amide dimer out-of-plane shear. (c) Aromatic ring system quadrant out-of-plane bend, dimer in-phase + primary amide dimer in-phase, out-of-plane twist. (d) Aromatic ring system out-of-plane fold in thirds, dimers out-of-phase + primary amide dimer out-of-plane shear. (e) Aromatic ring system out-of-plane fold in thirds, dimers in-phase + primary amide dimer out-of-plane bend.

ring bend modes (Figs. 4b and 4c) occur at 170 and 118 cm^{-1} , respectively. The relative phase of the two CBZ ring-system vibrations can also differ, resulting in additional degenerate calculated modes. Table I summarizes the observed low-frequency Raman band frequencies, bandwidths, and the band assignments for CBZ in solution.

The vibrational modes for CBZ below 55 cm^{-1} are summarized in Fig. 5. Only one node (indicated by the dashed line) is present in the vibrational modes shown for the aromatic ring system (Figs. 5a–5c), which corresponds to a rotation of the aromatic ring that is also coupled to the primary amide in-plane rock or the out-of-plane shear. The last vibrational mode (Fig. 5d) involves an in-plane rotation of the aromatic ring system coupled with the primary amide in-plane rock. In more

isolated symmetric molecules, these vibrations would translate to simple rotations and would not be IR or Raman active. However, in the less symmetric solid-state crystalline environment, CBZ bands observed below 55 cm^{-1} can involve both the intramolecular vibrations depicted in Figs. 4 and 5 and the external (lattice) vibrations. Greater coupling of the intermolecular and low-energy intramolecular motions for larger aromatic organics are more likely to occur in the 130–55 cm^{-1} spectral region due to the spectral overlap of both the intramolecular and intermolecular vibrations.

Low-Frequency Raman Spectroscopy of Selected Crystalline Forms of Carbamazepine. Known crystalline forms of CBZ include the dihydrate and four anhydrous polymorphs (Forms I, II, III, and IV). Figure 6 (top) shows the packing diagrams of the two anhydrous

TABLE I. Summary of observed Raman bands for the carbamazepine dimer in chloroform solution in the 200–55 cm⁻¹ spectral region along with selected Raman band assignments.

Peak frequency (cm ⁻¹)	FWHH (cm ⁻¹)	Assignment	Figure depicting intramolecular vibrational mode	Number of modes
170	9.7	Aromatic ring system sextant out-of-plane bend + primary amide dimer out-of-plane shear	4b	1
		Aromatic ring quadrant out-of-plane fold (accordion) + primary amide dimer in-plane rock	4a	2
118	12.4	Aromatic ring quadrant out-of-plane bend + primary amide dimer out-of-plane twist	4c	2
91	32.6	Aromatic ring third-circle out-of-plane fold dimer rings out-of-phase (butterfly wing bend) + primary amide dimer out-of-plane shear	4d	1
58	23.1	Aromatic ring third circle out-of-plane fold (butterfly wing bend) + primary amide dimer out-of-plane bend or shear	4e	2

polymorphs (Forms II and III) and the pseudo-polymorphic dihydrate form examined in this study. The unit cell parameters for all three crystalline forms are summarized in Table S1. Two important molecular interactions

in the CBZ solid-state forms are hydrogen bonding involving (1) the primary amide group and (2) π - π stacking interactions between the aromatic rings. In all three crystalline forms depicted in Fig. 6, the CBZ

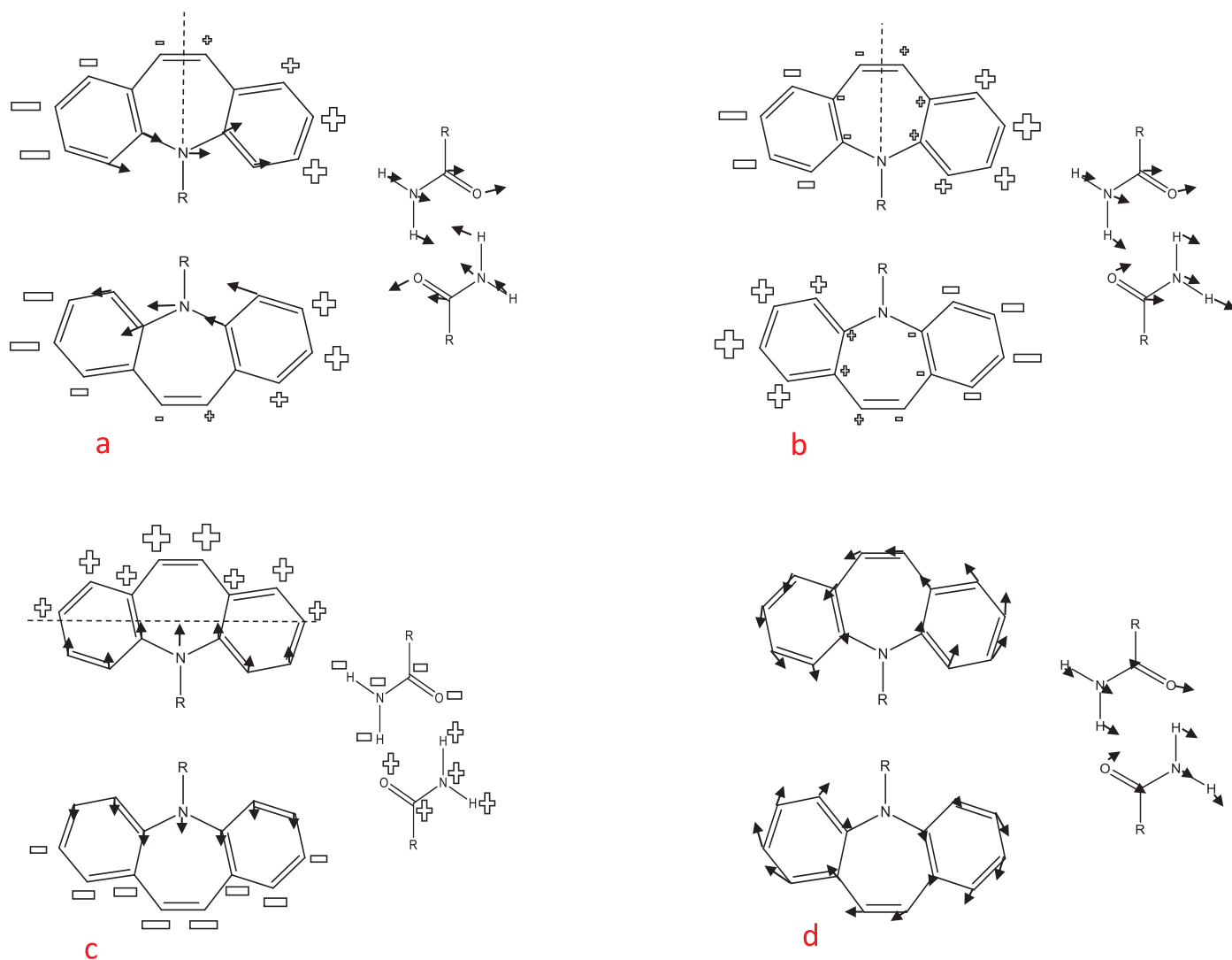


FIG. 5. Depiction of selected normal mode vibrations of CBZ dimer in the low-frequency Raman region of 55–10 cm⁻¹. A standing-wave description is used for the aromatic bending and folding vibrations where the nodes are highlighted with dashed lines. The vibrational modes are shown from highest to lowest calculated frequency. **(a)** Aromatic ring system semi-circle out-of-plane bend with a ring amino group translation + primary amide dimer in-plane rock. **(b)** Aromatic ring system semi-circle out-of-plane bend + primary amide dimer in-plane rock. **(c)** Aromatic ring system semi-circle fold + primary amide dimer out-of-plane shear. **(d)** Aromatic ring rotation + primary amide dimer in-plane rock.

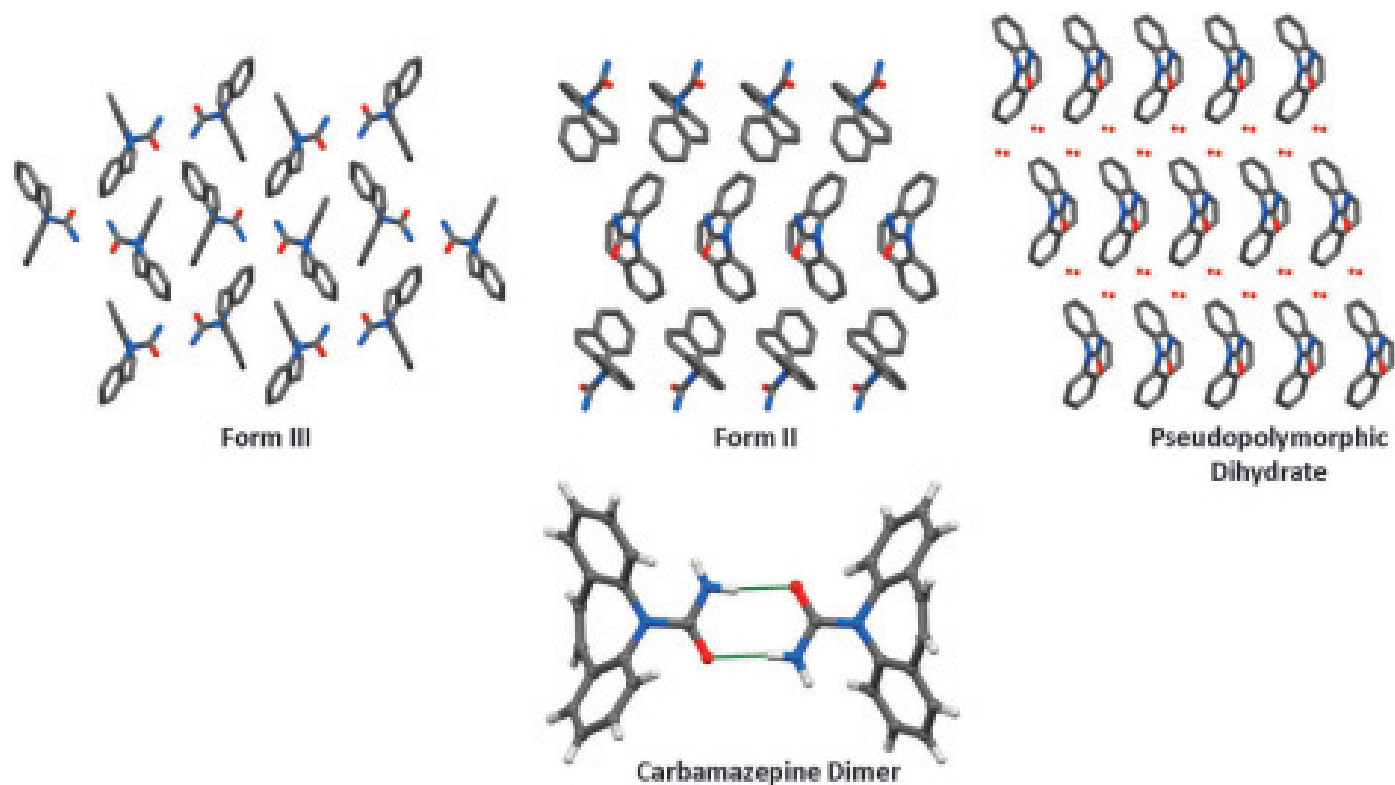


FIG. 6. (Top row) The packing diagrams of two CBZ anhydrous polymorphs (Forms II and III) and the pseudo-polymorphic dihydrate form, illustrating the π - π stacking geometries of the aromatic rings. The hydrogen atoms are omitted for clarity. The water molecules in the pseudo-polymorphic dihydrate are indicated by two red spheres per water molecule. (Bottom row) The hydrogen-bonded dimer present in all three CBZ crystalline forms.

molecules form a centrosymmetric amide–amide dimer involving a strong $\text{NH} \dots \text{O}(=\text{C})$ hydrogen bond. This hydrogen-bonding interaction can also be observed in the highly concentrated (100.5 mg/mL) solution phase of CBZ shown in Fig. 3. The hydrogen-bonded CBZ dimer structure is highlighted in Fig. 6 (bottom) and exhibits a distinctive bowtie geometry. Both the Form II and the pseudo-polymorphic dihydrate crystal form demonstrate a similar off-set ring-stacking configuration that differs significantly from the Form III aromatic ring-stacking geometry. Carbamazepine Form II demonstrates a higher, R-trigonal ($R\bar{3}$) symmetry than that of the P-monoclinic ($P2_1/c$) crystal symmetries shared by the Form III and dihydrate crystalline forms.

Figure 7 shows the low-frequency Raman spectra of CBZ Forms III and II (Figs. 7a and 7c) and the pseudo-polymorphic dihydrate crystalline form (Fig. 7b) in the 200–10 cm^{-1} spectral region. Tables II–IV summarize the observed peaks and their full width half-heights (FWHMs) for these three forms. The CBZ peaks and their FWHMs were determined using a Gaussian fit peak-resolution methodology. In general, all three low-frequency Raman spectra show differences as a function of the crystalline form. However, Form III (Fig. 7a) and the pseudo-polymorphic dihydrate (Fig. 7b) both have P-monoclinic symmetry and display similar spectral features in the low-frequency Raman spectra regions 200–135 and 95–35 cm^{-1} . Despite the similar π - π off-set ring-stacking interactions illustrated in Fig. 6 (top), the low-frequency Raman spectra of the Form II (Fig. 7c) and the pseudo-polymorphic dihydrate (Fig. 7b) are quite different, with

only slight similarities observed in the 135–95 cm^{-1} spectral region.

An examination of the CBZ Form II low-frequency Raman spectrum in Fig. 7c reveals four distinct clusters of Raman bands. These can be classified into four spectral regions: 200–150, 150–100, 100–55, and 55–10 cm^{-1} . As summarized in Table II, the average frequencies of all bands from these spectral regions are 166, 116, 79, and 25 cm^{-1} , with an average FWHM of 8.9, 14, 12.9, and 5.3 cm^{-1} , respectively. The agreement between the CBZ Form II solid average frequencies and FWHM and the data for CBZ in solution (Table I) is excellent in the 200–100 cm^{-1} spectral region. However, the agreement is not as strong below 100 cm^{-1} , including a three- to fourfold improvement in the average FWHM for the solid-state data. This dramatic change is most likely a consequence of the collective (long-range, ordered) nature of the vibrations (phonons) in the crystalline solid.

A comparison of the low-frequency Raman spectra of the CBZ Form II, Form III, and pseudo-polymorphic dihydrate reveals several useful trends. First, the average frequencies and FWHMs for CBZ Form III and the pseudo-polymorphic dihydrate shown in Tables III and IV, respectively, are essentially identical for the three spectral regions between 200 and 55 cm^{-1} . Second, these average frequencies and average FWHMs are significantly different than those found for Form II. These results are consistent with the identical crystalline symmetry (P-monoclinic) for the CBZ pseudo-polymorphic dihydrate and Form III and the different symmetry (R-trigonal) for Form II. Last, the largest systematic

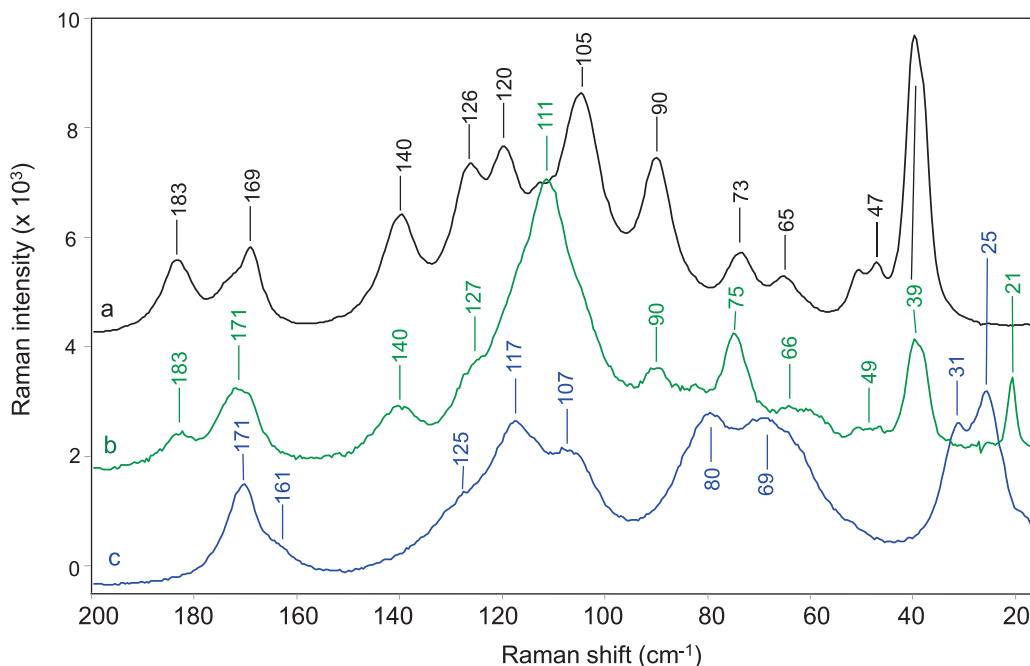


FIG. 7. The low-frequency Raman spectrum of three CBZ crystalline forms. All three Raman spectra were measured at room temperature (273° K). The spectra are off-set for clarity. (a) Form III. (b) Pseudo-polymorphic dihydrate form. (c) Form II.

differences among the three CBZ crystalline forms are observed in the 55–10 cm^{-1} spectral region. We expect this spectral region to be dominated by contributions from external (lattice) vibrations. Form III has an average frequency of 45 cm^{-1} , the pseudo-polymorphic dihydrate has 36 cm^{-1} , and Form II has 25 cm^{-1} . The spectral bandwidth (FWHM) of the low-frequency Raman bands in this spectral region is the narrowest, thereby further improving the spectral specificity.

Low-Frequency Raman Spectroscopy of Isostructural Apixaban Hemi-Diacid Cocrystals. Because external (lattice) vibrations contribute significantly to the low-frequency Raman spectra of APIs, the Raman bands in the 200–10 cm^{-1} region are expected to be highly correlated with the crystal structure of the molecule. This contributes to the clear differentiation of the low-frequency Raman spectra of different crystalline forms of CBZ. Conversely, an API with different diacid cocrystals, but with identical molecular-packing, aromatic ring-stacking and hydrogen-bonding interactions

should have little or no differentiation in the low-frequency Raman spectral region. The unit cell parameters of such isostructural crystalline systems should be almost identical. Differences are expected in the conventional IR and Raman spectra, reflecting the intramolecular vibrations and the molecular structures of the cocrystals.

Known crystalline forms of apixaban include a pseudo-polymorphic dihydrate; an anhydrous form; and at least three different hemi-diacid cocrystals, including hemi-fumaric acid, hemi-succinic acid, and hemi-D,L-malic acid. Because the cocrystals of apixaban are isostructural, the molecules adopt the same symmetry and exhibit very similar molecular packing in the solid state. All three apixaban diacid cocrystals exhibit P-monoclinic ($P2_1/n$) symmetry and display the identical molecular packing, aromatic ring stacking, and hydrogen bonding, as depicted in Fig. 8. Because of this, the unit cell

TABLE II. Summary of observed Raman bands in the 200–10 cm^{-1} low-frequency spectral region of carbamazepine Form II.^a

Peak frequency (cm^{-1})	FWHM (cm^{-1})	Relative peak height ^b	Comments	Average frequency and FWHM ^c (cm^{-1})	
170.7	8.9	0.54	Clearly defined peak	166	8.9
161.1	8.8	0.12	Shoulder		
125.1	21.9	0.54	Shoulder	116	14.0
116.8	9.2	0.54	Clearly defined peak		
106.8	10.8	0.62	Clearly defined peak	79	12.9
86.3	9.5	0.25	Shoulder		
80.4	8.7	0.52	Clearly defined peak		
68.9	20.4	1.00	Clearly defined peak		
31.3	7	0.68	Clearly defined peak	25	5.3
25.2	5.3	0.77	Clearly defined peak		
19	3.6	0.21	Shoulder		

^a This form belongs to the trigonal crystal system (space group $R\bar{3}$).

^b Peak height is relative to the most intense band observed at $\sim 69 \text{ cm}^{-1}$.

^c Carbamazepine spectrum is divided into four general regions: 200–150, 150–100, 100–55, and 55–10 cm^{-1} .

TABLE III. Summary of observed Raman bands in the 200–10 cm⁻¹ low-frequency spectral region of carbamazepine Form III.^a

Peak frequency (cm ⁻¹)	FWHH (cm ⁻¹)	Relative peak height ^b	Comments	Average frequency and FWHH ^c (cm ⁻¹)	
183.2	7.7	0.24	Clearly defined peak	173	6.8
173.2	6.7	0.15	Shoulder		
168.8	3.7	0.17	Clearly defined peak		
167.8	9	0.08	Slight shoulder	125	7.1
144.5	7.2	0.08	Slight shoulder		
139.7	6.4	0.34	Clearly defined peak		
126.4	7.2	0.56	Clearly defined peak		
119.6	6.0	0.56	Clearly defined peak		
113.2	6.9	0.42	Shoulder	75	7.0
104.8	8.8	0.82	Clearly defined peak		
90	5.8	0.42	Clearly defined peak		
85.3	11.9	0.20	Slight shoulder		
73.5	7.0	0.24	Clearly defined peak		
65.1	6.5	0.15	Clearly defined peak		
59.9	4	0.03	Very slight shoulder		
52.8	8.9	0.06	Very slight shoulder	45	6.0
51.1	2.7	0.10	Clearly defined peak		
46.9	5.4	0.20	Clearly defined peak		
39.4	4.7	1.00	Clearly defined peak		
35.4	8.3	0.09	Shoulder		

^a This form belongs to the monoclinic crystal system (space group $P2_1/c$).

^b Peak height is relative to the most intense band observed at ~ 39 cm⁻¹.

^c Carbamazepine spectrum is divided into four general regions: 200–150, 150–100, 100–55, and 55–10 cm⁻¹.

parameters (see Table SII) for the fumaric, succinic, and malic acid cocrystals are almost identical. All three diacid molecules are located in a channel in the same location in the molecular crystal, along the *a*-axis, and link with the API molecule through hydrogen bonding involving the apixaban primary amide carbonyl group and the carboxylic acid hydroxyl group.

Figure 9 shows the low-frequency Raman spectra of the three cocrystals of the same cocrystalline form of apixaban. Table V summarizes the observed peaks and their FWHHs for the three isostructural apixaban diacid cocrystal forms. Note that the low-frequency Raman spectra of all three apixaban cocrystals are almost identical. The high-frequency Raman spectra (not shown) of all three apixaban cocrystals are also quite

similar, but they display some differences as a result of the different cocrystal molecules (fumaric acid, succinic acid, or malic acid) in the molecular crystals. The differences in the spectral behavior in these two Raman spectral regions occur because the low-frequency Raman spectra derive in part from lattice vibrations of the apixaban crystalline form while the higher-frequency Raman spectra access fundamental molecular vibrations reflecting the molecular structure. The highly similar low-frequency Raman spectra of the apixaban diacid cocrystal forms occur because the spectral region has significant contributions from external (lattice) vibrations, which are highly correlated with the crystal structure of the molecule.

TABLE IV. Summary of observed Raman bands in the 200–10 cm⁻¹ low-frequency spectral region of carbamazepine pseudo-polymorphic dihydrate form.^a

Peak frequency (cm ⁻¹)	FWHH (cm ⁻¹)	Relative peak height ^b	Comments	Average frequency and FWHH ^c (cm ⁻¹)	
182.6	7.7	0.09	Clearly defined peak	177	7.2
171.5	6.7	0.27	Clearly defined peak		
145.1	6.3	0.06	Slight shoulder		
139.9	7.1	0.18	Clearly defined peak	124	6.7
126.8	6.3	0.27	Shoulder		
122.7	5.4	0.20	Slight shoulder		
117.9	6.8	0.54	Shoulder		
111.3	7.6	1.00	Clearly defined peak		
104.7	7.2	0.50	Shoulder	76	7.1
98.2	7.7	0.25	Slight shoulder		
89.9	8.2	0.33	Clearly defined peak		
82.3	6.2	0.23	Clearly defined peak		
74.8	6.6	0.44	Clearly defined peak		
66.2	9.6	0.17	Overlapped peak		
61.2	6.0	0.07	Overlapped peak		
57.6	5.5	0.09	Overlapped peak	36	5.7
48.8	9.5	0.11	Clearly defined peak		
39.2	5.0	0.43	Clearly defined peak		
20.7	2.6	0.24	Clearly defined peak		

^a This form belongs to the monoclinic crystal system (space group $P2_1/c$).

^b Peak height is relative to the most intense band observed at ~ 111 cm⁻¹.

^c Carbamazepine spectrum is divided into four general regions: 200–150, 150–100, 100–55, and 55–10 cm⁻¹.

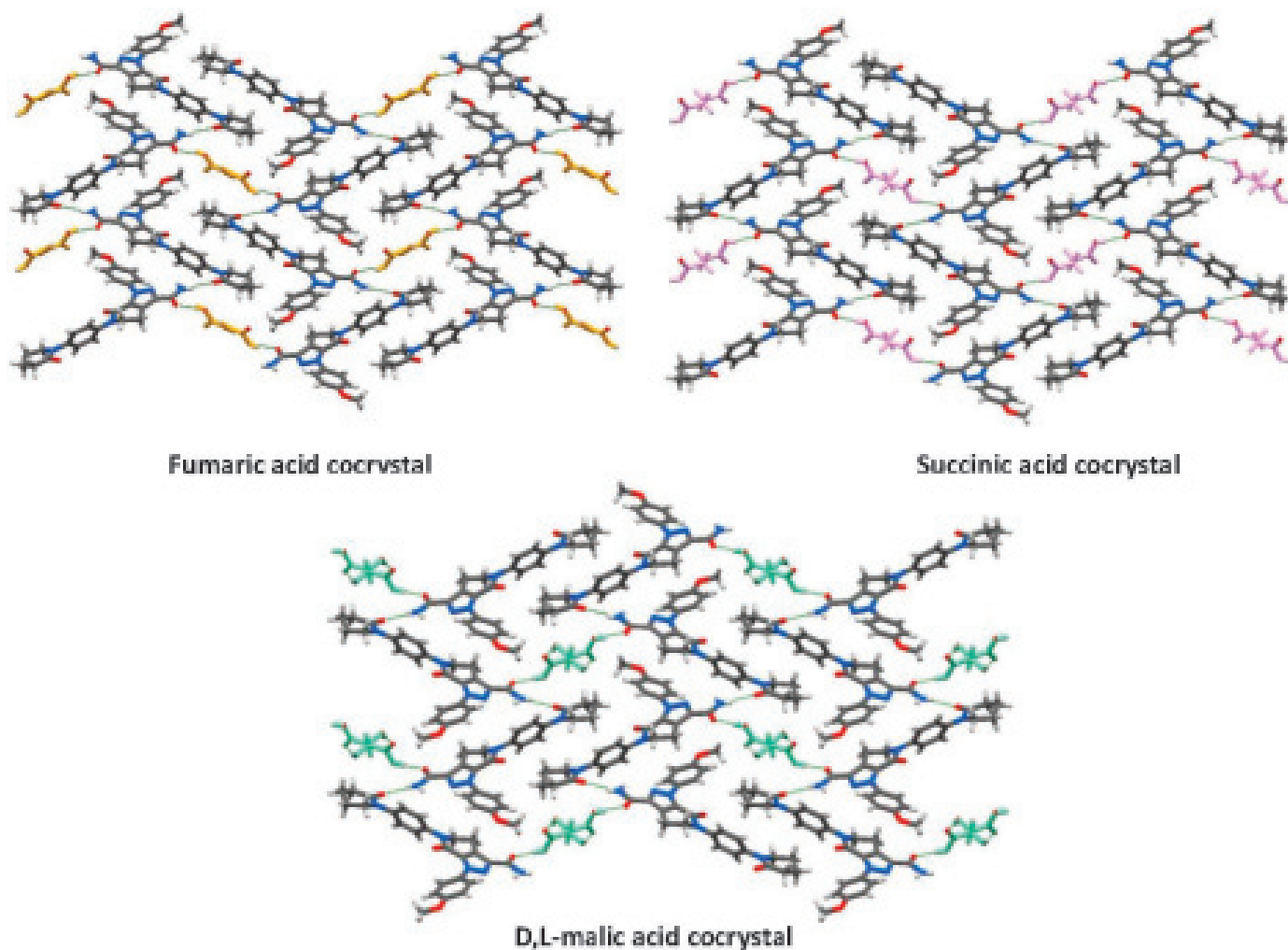


FIG. 8. Packing diagrams of apixaban cocrystals with fumaric, succinic, and D,L-malic acids. All the structures adopt the same overall packing and hydrogen-bond synthons. Apixaban molecules are drawn with element-specific colors, and the coformer molecules are drawn in orange (fumaric acid), magenta (succinic acid), or green (D,L-malic acid).

Low-Frequency Raman Spectroscopy as a Probe of Disorder: Theophylline and Caffeine. Low-frequency Raman spectroscopy is a potential probe of phase transformations, orientational disorder, and crystallization.^{18–22} Both the spectral linewidths and the peak position, as well as the selection rules, are expected to provide important information. Thus, a comparison of structurally similar theophylline and caffeine provides an initial model for the potential application of low-frequency Raman spectroscopy as a probe of solid-state crystalline disorder.

Theophylline has been shown to crystallize in either a monohydrate form or in one of five anhydrous polymorphs (Forms I, II, III, IV, and V).³⁹ Figure 10 shows the packing diagrams of the commercially available anhydrous Form II and the pseudo-polymorphic monohydrate examined in this study. The theophylline anhydrous Form II has a higher degree of symmetry (P-orthorhombic [*Pna2*₁]) than the pseudo-polymorphic monohydrate crystalline form (P-monoclinic [*P2*₁/*n*]). The unit cell parameters for both crystalline forms are summarized in Table SIII. Both crystal forms of theophylline display an ordered arrangement of molecules in which the hydro-

gen-bonded network of theophylline molecules are stacked on top of one another to form π – π interactions between the aromatic rings. The functional groups involved in the hydrogen bonding differ for the two different crystalline forms. In the anhydrous Form II, the hydrogen bonding involves the amine (NH) groups and N atoms of the five-member purine ring. Here the theophylline molecules are packed into infinite zig-zag arrays through the NH ... N hydrogen bonds. In the pseudo-polymorphic hydrate form, NH ... O bonds involving the NH group of the purine and one of the lactam carbonyl groups result in the formation of molecular dimers. These theophylline dimers are further linked by the water molecules located in the channels of the crystal through an OH ... N hydrogen bond involving a purine-ring N atom. One of the theophylline methyl groups in the monohydrate form displays dynamic disorder.

The low-frequency Raman spectra of the theophylline pseudo-polymorphic monohydrate and anhydrous Form II are shown in Figs. 11a and 11b, respectively. Table VI summarizes the peak frequencies, FWHHs, and relative peak intensities for both forms. Analogous to our

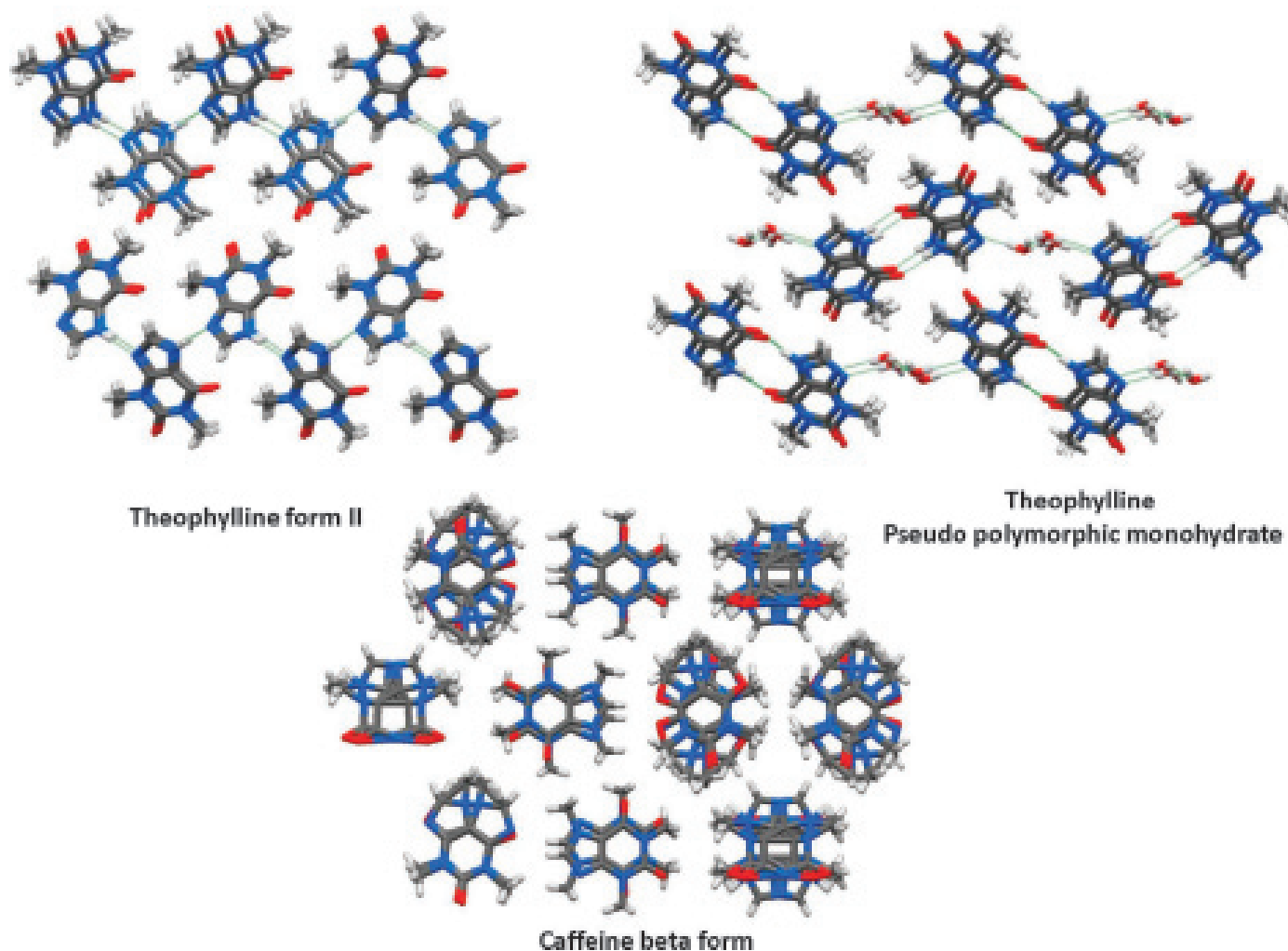


FIG. 10. Crystal structures of theophylline anhydrous Form II, theophylline pseudo-polymorphic monohydrate form, and caffeine anhydrous beta form. In contrast to the two forms of theophylline, anhydrous caffeine lacks strong hydrogen bonds (due to the absence of NH groups) and shows extensive positional molecular disorder.

interactions are the dominant force between the caffeine molecules. As shown in Fig. 10, the caffeine molecules are stacked into columns along the *c*-axis and there is positional disorder of the molecules. The low-frequency Raman spectrum of the caffeine anhydrous beta form is shown in Fig. 11c.

The low-frequency Raman spectrum of anhydrous caffeine shows several broad spectral bands below $\sim 60\text{ cm}^{-1}$. Clearly distinguished peaks are observed at 38 and 19 cm^{-1} . Table VII summarizes the observed peaks, their spectral bandwidths (FWHMs), and relative intensities. Unlike CBZ, apixaban, or theophylline, caffeine exhibits no spectral features in the region $200\text{--}60\text{ cm}^{-1}$. In addition, the FWHMs of the caffeine bands are significantly greater than those observed below 60 cm^{-1} for the crystalline forms of CBZ, apixaban, and theophylline. This behavior most likely derives from the considerable positional and dynamic disorder displayed by caffeine and demonstrates the potential of low-frequency Raman spectroscopy to be used as a probe of disordered states.^{19,21}

A comparison of the low-frequency Raman spectra of the theophylline anhydrous Form II (Fig. 11b) and the

caffeine anhydrous beta form (Fig. 11c) shows some similarities in the peak positions below 60 cm^{-1} , which have been ascribed to the similar molecular-packing arrangements.²¹ As shown in Fig. 10, both theophylline and caffeine have similar $\pi\text{--}\pi$ stacking arrangements. However, theophylline Form II exhibits higher symmetry than the caffeine anhydrous beta form. Computational studies are ongoing to more fully understand the low-frequency Raman spectra of APIs such as CBZ, apixaban, theophylline, and caffeine.

Application of Low-Frequency Raman Spectroscopy to Pharmaceutical Drug Products. The application of NIR spectroscopy and conventional IR and Raman spectroscopies to the analyses of APIs in pharmaceutical drug products must take into account potential interference from the often much more highly concentrated excipients. Increasingly, this potential interference has become a factor as more potent APIs, requiring that lower dosages be introduced. Conventional Raman spectroscopy does provide a greater sensitivity to aromatic APIs than to most nonaromatic excipients,³² but the possible interference from crystalline excipients

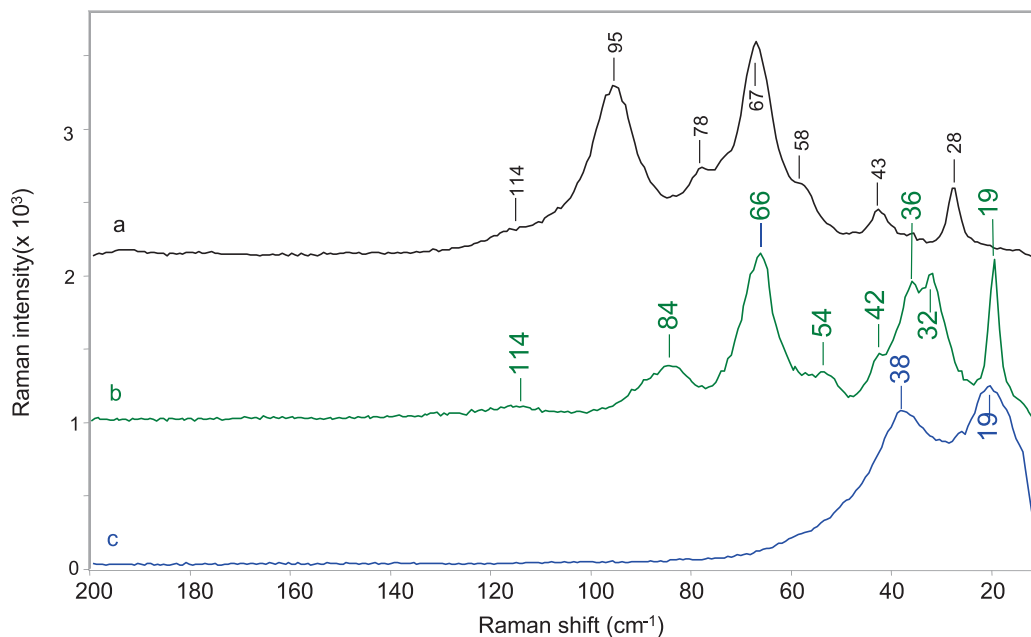


FIG. 11. Low-frequency Raman spectrum of two crystalline forms of theophylline and one form of caffeine. The spectra are offset for clarity. (a) Theophylline pseudo-polymorphic monohydrate form. (b) Theophylline anhydrous Form II. (c) Caffeine anhydrous beta form. The chemical structures of caffeine and theophylline are nearly identical, differing by only a methyl group on the imidazole N atom. The theophylline crystalline forms are characterized by strong intermolecular hydrogen bonding not present in caffeine. The caffeine crystalline structure includes orientational disorder, demonstrated by the broadening of the low-frequency Raman bands.

TABLE VI. Summary of observed Raman bands in the 200–10 cm^{-1} low-frequency spectral region of theophylline anhydrous Form II and pseudo-polymorphic monohydrate form.^a

Anhydrous Form II			Pseudo-polymorphic monohydrate		
Peak frequency (cm^{-1})	FWHM (cm^{-1})	Peak height ^b	Peak frequency (cm^{-1})	FWHM (cm^{-1})	Peak height ^b
116.4	8.5	0.03	114.4	12.0	0.14
			101.2	10.9	0.37
90.2	7.1	0.37	94.8	8.7	0.99
83.6	8.0	0.37			
73.9	9.1	0.26	74.6	20.3	0.67
65.7	5.3	1.00	66.8	6.12	1.00
60.9	6.0	0.33	58.4	9.73	0.44
53.6	8.8	0.35			
41.9	6.9	0.46	42.3	5.2	0.27
36.1	5.0	0.85	36.8	3.9	0.07
31.8	4.3	0.64			
29.1	7.2	0.45	27.6	2.7	0.36
19.4	2.4	0.78			

^a The anhydrous Form II belongs to the orthorhombic crystal system (space group $Pna2_1$), and the pseudo-polymorphic monohydrate belongs to the monoclinic crystal system (space group $P2_1/n$).

^b Peak height is relative to the most intense band observed at $\sim 66 \text{ cm}^{-1}$.

in the low-frequency Raman spectral region has not yet been well characterized.

Figure 12a compares the low-frequency Raman spectra of the CBZ crystalline Form II to some common nonaromatic excipients: sucrose, lactose, and Avicel (microcrystalline cellulose (MCC)). Both the sucrose and lactose samples were highly crystalline, but the Avicel sample was predominantly disordered crystalline cellulose with some in an amorphous phase. All samples were collected using identical sampling conditions and laser power, enabling an approximate comparison of Raman intensities. The low-frequency Raman spectra overlay of the excipients and CBZ (Fig. 12a) uses a common intensity scale that demonstrates the signifi-

TABLE VII. Summary of observed Raman bands in the 200–10 cm^{-1} low-frequency spectral region of caffeine anhydrous beta form.^a

Peak frequency (cm^{-1})	FWHM (cm^{-1})	Peak height ^b	Comments
46.5	30.4	0.28	Asymmetric peak/shoulder
43.9	12.6	0.25	Asymmetric peak/shoulder
37.8	9.0	0.59	Peak
27.9	13.1	0.71	Shoulder
19.2	8.7	1.00	Peak
14.1	4.2	0.40	Shoulder

^a This form belongs to the monoclinic crystal system (space group $C2/c$).

^b Peak height is relative to the most intense band observed at $\sim 19 \text{ cm}^{-1}$.

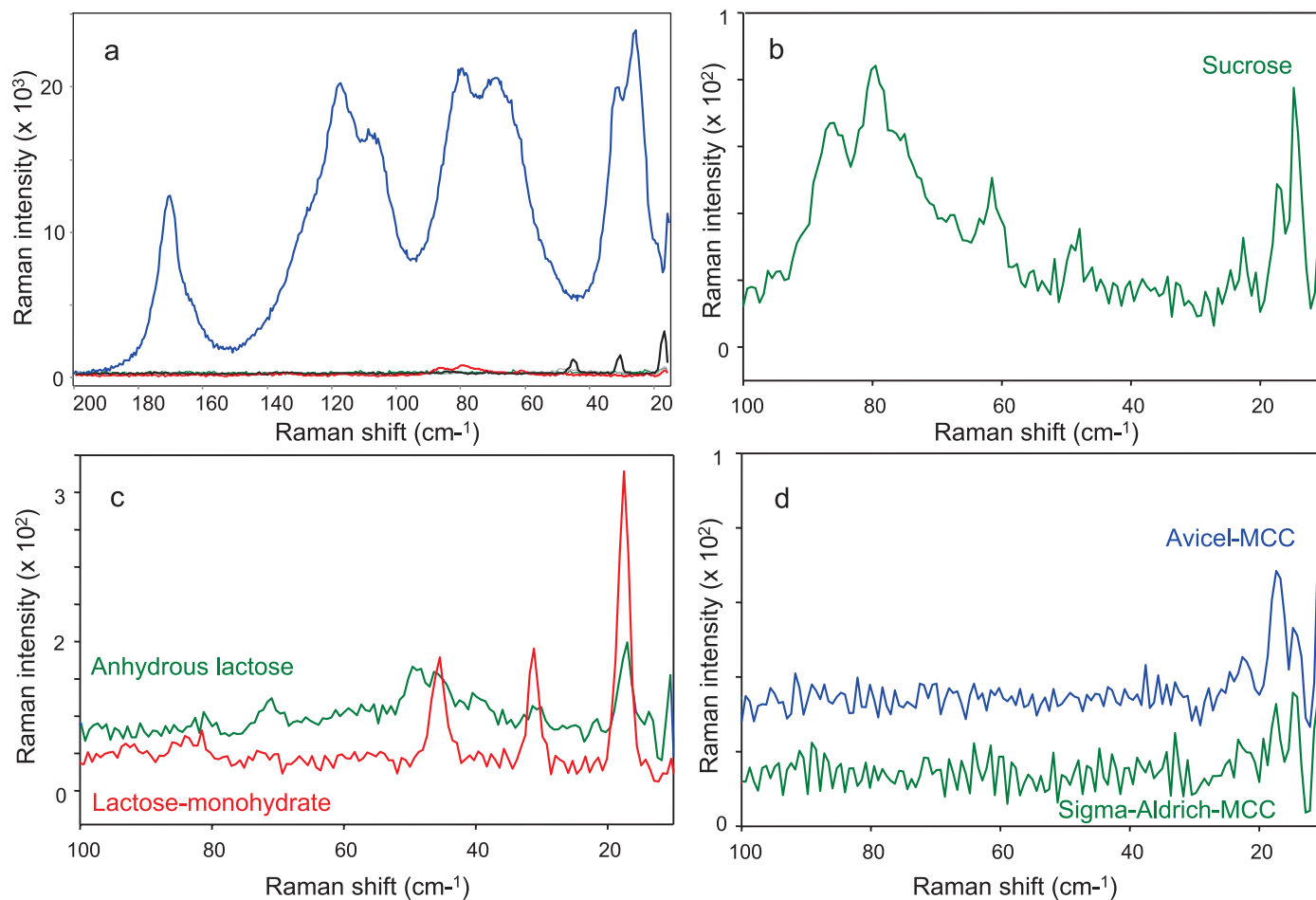


FIG. 12. Low-frequency Raman spectrum of CBZ and selected organic excipients. Both the API (i.e., CBZ) and excipients were measured under the same experimental conditions. (a) Carbamazepine Form II (blue trace) and four common excipients with the same intensity axis: sucrose (red), lactose monohydrate (black), anhydrous lactose (gray), and Avicel (green). (b–d) Low-frequency Raman spectra of the excipients with expanded intensity axes to illustrate the spectral features. The intensity observed for the aromatic API vibrations are more than an order of magnitude greater than the common organic excipients investigated.

cantly lower Raman intensities observed for the nonaromatic excipients relative to the aromatic CBZ API. As illustrated in Figs. 12b–12d, the low-frequency Raman spectra are unique to each excipient. Different polymorphic forms of lactose demonstrate that the low-frequency Raman spectra are capable of differentiating among the different crystalline forms of the excipients. In general, the low-frequency Raman bands of the aromatic APIs show approximately a 10- to 20-fold greater intensity than do typical pharmaceutical excipients. This difference in the intensity of the low-frequency Raman bands of aromatic APIs and saturated organic excipients is due to three factors: (1) the aromatic APIs are more polarizable than the nonaromatic excipients, resulting in greater Raman intensity for aromatic APIs;³² (2) the intensity of low-frequency Raman bands of the aromatic APIs are two to five times greater than their most intense fingerprint band;³⁴ and (3) the intensity of the low-frequency Raman bands of most excipients exhibit equal or weaker intensity than the most-intense higher-frequency Raman bands ($4000\text{--}400\text{ cm}^{-1}$). Because of these three factors, low-frequency Raman spectroscopy

is particularly well suited for the characterization of APIs in pharmaceutical drug products.

CONCLUSION

We have applied recent innovations in filter technology that enable the measurement of high-quality, low-frequency Raman spectra in the $200\text{--}10\text{ cm}^{-1}$ region to selected APIs and excipients. In pharmaceutical drug substances, the low-frequency Raman spectral region of organic molecular crystals typically includes contributions from both molecular vibrations and crystal lattice modes. The extension of Raman spectroscopy to include this spectral region is of particular interest because, compared to THz spectroscopy, low-frequency Raman spectroscopy requires no sample preparation and provides highly flexible sampling options. The simultaneous use of both the conventional and low-frequency spectral regions should provide significant improvement in the solid-state specificity of Raman spectroscopy.

This investigation demonstrates that the low-frequency Raman spectra of large aromatic species typical of APIs provide remarkably intense bands below 200 cm^{-1} with complex spectral features. The most intense bands

in the Raman spectra of aromatic APIs are found in this spectral region and are 10- to 20-fold more intense than those observed for saturated organic excipients. The low-frequency Raman bands provide a highly sensitive probe of the polymorphic forms of aromatic APIs. This low-frequency Raman spectral region can be considered a second fingerprint region that is specific for crystalline structure, crystalline disorder, and amorphous states.

We used this new filter technology to study the low-frequency Raman spectroscopy of four APIs with rigid ring structures: CBZ, apixaban diacid isostructural cofomers, theophylline, and caffeine. The evaluation of the Raman spectra of CBZ in a chloroform solution demonstrates that, for large complex aromatic molecular systems, several distinct intramolecular vibrations can be observed in the region 200–50 cm^{-1} , with a larger relative intensity than observed in the higher-frequency fingerprint region. We compared these results to selected CBZ solid crystalline forms, which are much more complex and include lattice vibrations. In the spectra for CBZ, theophylline, and apixaban, the narrowest bandwidths were found to occur below 50 cm^{-1} , which include the largest contributions from lattice modes, making them ideal for detecting differences in unit cell packing and crystalline structure. Finally, we found that the known positional and dynamic disorder of the caffeine anhydrous beta form resulted in significantly greater bandwidths than were displayed by the other three, more highly crystalline APIs and demonstrated the potential use of low-frequency Raman spectroscopy as a probe of amorphous and disordered states. Because the Raman vibrations of aromatic APIs are significantly more intense in this spectral region than are those observed for saturated organic excipients, low-frequency Raman is well suited for monitoring the crystalline and amorphous states of the API in both drug substances and drug products.

Future development of the low-frequency Raman technique will require an improved understanding of the relationship between crystalline structure and the low-frequency vibrational spectrum. Applying existing computation techniques for calculating the solid-state vibrational spectra will enhance our understanding of the molecular and lattice vibrations that give rise to the useful group frequencies observed in the low-frequency Raman spectra of aromatic APIs.

ACKNOWLEDGEMENTS

We gratefully acknowledge the Bristol-Myers Squibb Company for providing the resources needed to carry out this study and for permission to publish this work. We also acknowledge Jason McClure of Princeton Instruments for useful discussions.

SUPPLEMENTAL MATERIAL

All supplemental materials mentioned in the text, including three tables of the selected API crystalline forms unit cell parameters and densities, and four figures summarizing the PXRD confirmation of the crystalline forms, can be found in the online version of the journal at <http://www.s-a-s.org>.

1. S.R. Byrn, R.R. Pfeiffer, J.G. Stowell. "Drugs as Molecular Solids". In: *Solid-State Chemistry of Drugs*. West Lafayette, IN: SSCI, 1999. 2nd ed., Chap. 1, pp. 5-29.
2. A. Burger. "The Relevance of Polymorphism". In: D.D. Breimer, P. Speiser, editors. *Topics in Pharmaceutical Sciences: Proceedings*

- of the International Congress of Pharmaceutical Sciences of FIP held in Vienna, Austria, September 7-11, 1981. Amsterdam: Elsevier/North Holland Biomedical Press, 1981. Pp. 347-359.
3. J. Bernstein. "Polymorphism in Molecular Crystals". In: J. Bernstein, editor. *Polymorphism in Molecular Crystals: IUCr Monographs on Crystallography*. Oxford: Oxford University Press, 2002. Pp. 1–28.
 4. G.P. Stahly. "A Survey of Cocrystals Reported Prior to 2000". *Cryst. Growth Des.* 2009. 9(10): 4212-4229.
 5. S. Aitipamula, R. Banerjee, A.K. Bansal, K. Biradha, M.L. Cheney, A.R. Choudhury, G.R. Desiraju, A.G. Dikundwar, R. Dubey, N. Duggirala, P.P. Ghogale, S. Ghosh, P.K. Goswami, N.R. Goud, R.F.K.R. Jetti, P. Karpinski, P. Kaushik, D. Kumar, V. Kumar, B. Moulton, A. Mukherjee, G. Mukherjee, A.S. Myerson, V. Puri, A. Ramanan, T. Rajamannar, C.M. Reddy, N. Rodriguez-Hornedo, R.D. Rogers, T.N.G. Row, P. Sanphui, N. Shan, G. Shete, A. Singh, C.C. Sun, J.A. Swift, R. Thaimattam, T.S. Thakur, R.K. Thaper, S.P. Thomas, S. Tothadi, V.R. Vangala, N. Variankaval, P. Vishweshwar, D.R. Weyna, M.J. Zaworothko. "Polymorphs, Salts, and Cocrystals: What's in a Name". *Cryst. Growth Des.* 2012. 12(5): 2147-2152.
 6. P.J. Larkin. *Infrared and Raman Spectroscopy: Principles and Spectral Interpretation*. New York: Elsevier, 2011.
 7. B.C. Smith. *Infrared Spectral Interpretation: A Systematic Approach*. Boca Raton, FL: CRC Press, 1998.
 8. A. Heinz, C.J. Strachan, K.C. Gordon, T. Rades. "Analysis of Solid-State Transformations of Pharmaceutical Compounds Using Vibrational Spectroscopy". *J. Pharm. Pharmacol.* 2009. 61(8): 971-988.
 9. D.H. Igo, P. Chen. "Vibrational Spectroscopy of Solid-State Forms—Applications and Examples". In: D.E. Pivonka, J.M. Chalmers, P.R. Griffiths, editors. *Applications of Vibrational Spectroscopy in Pharmaceutical Research and Development*. Chichester, UK: John Wiley and Sons, 2007. Pp. 293-308.
 10. K.A. Bakeev, Ed. *Process Analytical Technology: Spectroscopic Tools and Implementation Strategies for the Chemical and Pharmaceutical Industries*. Oxford: Blackwell Publishing, 2005.
 11. E.P.J. Parrott, B.M. Fischer, L.F. Gladden, J.A. Zeitler, P.U. Jepsen. "Terahertz Spectroscopy of Crystalline and Non-Crystalline Solids". In: K.-E. Peiponen, A. Zeitler, M. Kuwata-Gonokami, editors. *Terahertz Spectroscopy and Imaging*. Springer Series in Optical Sciences no. 171. New York: Springer, 2013. Pp. 191-227.
 12. C. Moser, F. Havermeier. "Ultra-Narrow Band Tunable Laserline Notch Filter". *Appl. Phys. B: Lasers Opt.* 2009. 95(3): 597-601.
 13. J. Carriere, R. Heyler, B. Smith. "Polymorph Identification and Analysis Using Ultralow-Frequency Raman Spectroscopy". *Spectroscopy*. 2013. 26(6): S44-S50.
 14. D.C. Smith, C. Carabatos-Nedelec. "Raman Spectroscopy Applied to Crystals: Phenomena and Principles, Concepts and Conventions". In: I.R. Lewis, H. Edwards, editors. *Handbook of Raman Spectroscopy: From the Research Laboratory to the Process Line*. New York: Marcel Dekker, 2001. Pp. 349-422.
 15. A.P. Ayala. "Polymorphism in Drugs Investigated by low Wavenumber Raman Scattering". *Vib. Spectrosc.* 2007. 45(2): 112-116.
 16. S. Al-Dulaimi, A. Aina, J. Burley. "Rapid Polymorph Screening on Milligram Quantities of Pharmaceutical Material Using Phonon-Mode Raman Spectroscopy". *CrystEngComm*. 2010. 12(4): 1038-1040.
 17. A. Hedoux, L. Paccou, Y. Guinet, J.F. Willart, M. Descamps. "Using the Low-Frequency Raman Spectroscopy to Analyze the Crystallization of Amorphous Indomethacin". *Eur. J. Pharm. Sci.* 2009. 38(2): 156-164.
 18. A. Hedoux, Y. Guinet, M. Descamps. "The Contribution of Raman Spectroscopy to the Analysis of Phase Transformations in Pharmaceutical Compounds". *Int. J. Pharm.* 2011. 417(1): 17-31.
 19. A. Hedoux, A.A. Decroix, Y. Guinet, L. Paccou, P. Derollez, M. Descamps. "Low- and High-Frequency Raman Investigations on Caffeine: Polymorphism, Disorder and Phase Transformation". *J. Phys. Chem. B*. 2011. 115(19): 5746-5753.
 20. A.P. Ayala, M.W.C. Caetano, S.B. Honorato, J. Mendes Filho, H.W. Siesler, S.N. Faudone, S.L. Cuffini, F.T. Martins, C.C.P. da Silva, J. Ellena. "Conformational Polymorphism of the Antidiabetic Drug Chlorpropamide". *J. Raman Spectrosc.* 2012. 43(2): 263-272.
 21. A. Hedoux, Y. Guinet, L. Paccou, F. Danede, P. Derollez. "Polymorphic Transformation of Anhydrous Caffeine upon Grinding

- and Hydrostatic Pressurizing Analyzed by Low-Frequency Raman Spectroscopy". *J. Pharm. Sci.* 2013. 102(2): 162-170.
22. S. Roy, B. Chamberlin, A.J. Matzger. "Polymorph Discrimination Using Low Wavenumber Raman Spectroscopy". *Org. Process Res. Dev.* 2013. 17(7): 976-980.
 23. C.J. Strachan, T. Rades, D.A. Newnham, K.C. Gordon, M. Pepper, P.F. Taday. "Using Terahertz Pulsed Spectroscopy to Study Crystallinity of Pharmaceutical Materials". *Chem. Phys. Lett.* 2004. 390(1): 20-24.
 24. G.M. Day, J.A. Zeitler, W. Jones, T. Rades, P.F. Taday. "Understanding the Influence of Polymorphism on Phonon Spectra: Lattice Dynamics Calculations and Terahertz Spectroscopy of Carbamazepine". *J. Phys. Chem. B.* 2006. 110(1): 447-456.
 25. M.D. King, W.D. Buchana, T.M. Korter. "Identification and Quantification of Polymorphism in the Pharmaceutical Compound Diclofenac Acid by Terahertz Spectroscopy and Solid-State Density Functional Theory". *Anal. Chem.* 2011. 83(10): 3786-3792.
 26. S.P. Delaney, D. Pan, M. Galella, S.X. Yin, T.M. Korter. "Understanding the Origins of Conformational Disorder in the Crystalline Polymorphs of Irbesartan". *Cryst. Growth Des.* 2012. 12(10): 5017-5024.
 27. D. Tomerini, G.M. Day. "Computational Methods for the Assignment of Vibrational Modes in Crystalline Materials". In: K.-E. Peiponen, A. Zeitler, M. Kuwata-Gonokami, editors. *Terahertz Spectroscopy and Imaging*. Springer Series in Optical Sciences no. 171. New York: Springer, 2013. Chap. 7, pp. 151-187.
 28. M. Born, K. Huang. *Dynamical Theory of Crystal Lattices*. New York: Oxford University Press, 1954.
 29. M. Schwoerer, H.C. Wolf. "Molecular and Lattice Dynamics in Organic Molecular Crystals". In: *Organic Molecular Solids*. Weinheim, Germany: Wiley-VCH, 2007. Chap. 5, pp. 89-124.
 30. M. Dracinsky, E. Prochazkova, J. Kessler, J. Sebestik, P. Matejka, P. Bour. "Resolution of Organic Polymorphic Crystals by Raman Spectroscopy". *J. Phys. Chem. B.* 2013. 117(24): 7297-7307.
 31. L. Hyang, A. Shabaev, S.G. Lambrakos, L. Massa. "Ground-State Features in the THz Spectra of Molecular Clusters of β -HMX". *Appl. Spectrosc.* 2012. 66(10): 1242-1248.
 32. D.E. Bugay, J.O. Henck, M.L. Longmire, F.C. Thorley. "Raman Analysis of Pharmaceuticals". In: D.E. Pivonka, J.M. Chalmers, P.R. Griffiths, editors. *Applications of Vibrational Spectroscopy in Pharmaceutical Research and Development*. Chichester, UK: John Wiley and Sons, 2007. Pp. 239-262.
 33. APEX2 User Manual, Version 1.27. Madison, WI: Bruker Advanced X-ray Solutions, 2005.
 34. K. Ohno, J. Kimura, Y. Yamakita. "Strong Raman Activities of Low-Frequency Vibrational Modes in Alkylbenzenes: Conformation Specific σ - π Interactions Between Alkyl Chain and Benzene Ring". *Chem. Phys. Lett.* 2001. 342(1): 207-219.
 35. N.N. Brandt, A. Yu. Chikishev, V.I. Dolgovskii, S.I. Lebedenko. "Laser Raman Spectroscopy of the Effect of Solvent on the Low-Frequency Oscillations of Organic Molecules". *Laser Phys.* 2007. 17(9): 1133-1137.
 36. O.F. Nielsen. "Low-Frequency Spectroscopic Studies and Intermolecular Vibrational Energy Transfer in Liquids". *Annu. Rep. Prog. Chem. C.* 1996. 93: 57-99.
 37. W.G. Rothschild, R.M. Cavagnat. "On the Characteristics of the Orientational Motion of Liquid Chloroform: A Mid- and Low-Frequency Raman Study". *J. Chem. Phys.* 1993. 99(11): 8922-8929.
 38. D. Lin-Vien, N.B. Colthup, W.G. Fateley, J.G. Grasselli. "Aromatic and Heteroaromatic Rings". In: *The Handbook of Infrared and Raman Characteristic Frequencies of Organic Molecules*. New York: Academic Press, 1991. Chap. 17, pp. 277-306.
 39. M.D. Eddleston, K.E. Hejczyk, E.G. Bithell, G.M. Day, W. Jones. "Determination of the Crystal Structure of a New Polymorph of Theophylline". *Chemistry*. 2013. 19(24): 7883-7888.
 40. G.D. Enright, V.V. Tersikh, D.H. Brouwer, J.A. Ripmeester. "The Structure of Two Anhydrous Polymorphs of Caffeine from Single-Crystal Diffraction and Ultrahigh-Field Solid-State ^{13}C NMR Spectroscopy". *Cryst. Growth Des.* 2007. 7(8): 1406-1410.